Production of vector mesons in the string + $^3P_0$ model of polarized quark fragmentation

A. Kerbizi,[1] X. Artru,[2] and A. Martin[1]

[1]*INFN Sezione di Trieste and Dipartimento di Fisica, Università degli Studi di Trieste, Via Valerio 2, 34127 Trieste, Italy*

[2]*Universit de Lyon, Institut de Physique des deux Infinis (IP2I Lyon), Universit Lyon 1 and CNRS, 4 rue Enrico Fermi, F-69622 Villeurbanne, France*

(Received 13 September 2021; accepted 19 November 2021; published 28 December 2021)

The production of vector mesons in the fragmentation process of polarized quarks is studied within the recursive string + $^3P_0$ model, improving a previous version of the model in which the production of pseudoscalar mesons only was considered. Two types of couplings of the vector meson to quarks are introduced, their coupling constants being the additional free parameters of the model. The angular distribution of the decay products of the polarized vector meson is deduced from the spin density matrix of the meson and the spin information is propagated along the fragmentation chain taking into account the entanglement of spin states. The new model is implemented in a stand alone Monte Carlo program utilized to investigate in detail kinematic distributions and transverse spin asymmetries. The sensitivity of these observables to the new free parameters is discussed and the Monte Carlo results are compared with experimental data on transverse spin asymmetries.

DOI: 10.1103/PhysRevD.104.114038

I. INTRODUCTION

The quark (and gluon) fragmentation process is one of the most intriguing and interesting phenomenon of quantum chromodynamics. It belongs to the soft (long-distance), nonperturbative domain and it is usually encoded in fragmentation functions (FFs). FFs are thought to be universal functions, i.e., common to all high energy collision processes producing jets of hadrons (for a review see Ref. [1]). The most studied FF is $D_{1q}^h(z, p_T)$ which describes the fragmentation of an unpolarized quark q in a not analyzed hadron h. The variable z is the fraction of the quark energy carried by the hadron and p_T is the transverse momentum of the hadron with respect to the quark momentum. The Q^2 dependence of the fragmentation functions is not considered in this work.

Particularly interesting is the spin-dependent fragmentation function $H_{1q}^{h\perp}(z, p_T)$ which describes the Collins effect in the fragmentation of a transversely polarized quark q in a not analyzed hadron [2]. The effect is an azimuthal distribution of the form

$$\frac{d^3N_h}{dz dp_T d\phi_h} \propto 1 + a^{q\uparrow\to h+X}|\mathbf{S}_T|\sin(\phi_h - \phi_S). \quad (1)$$

The angles ϕ_h and ϕ_S are, respectively, the azimuthal angles of the hadron transverse momentum and of the fragmenting quark transverse polarization $\mathbf{S}_T$ around the quark momentum. The combination $\phi_C = \phi_h - \phi_S$ is the Collins angle of the hadron and the amplitude $a^{q\uparrow\to h+X}$ of the $\sin\phi_C$ modulation for a fully polarized quark is the Collins analyzing power. It is conventionally written as $a^{q\uparrow\to h+X} = -p_T H_{1q}^{h\perp}/(zMD_{1q}^h)$, M being the hadrons mass.

The Collins FF appears, coupled to the transversity parton distribution function (transversity PDF) h_1^q, in the so-called Collins asymmetry in semi-inclusive deep inelastic scattering (SIDIS) off transversely polarized nucleons. Neglecting the intrinsic quark transverse momentum, the asymmetry can be written as

$$A_{\text{Coll}} = \frac{\sum_q e_q^2 h_1^q \times a^{q\uparrow\to h+X} D_{1q}^h}{\sum_q e_q^2 f_1^q \times D_{1q}^h}, \quad (2)$$

where $q = u, d, s, \bar{u}, \bar{d}$ or $\bar{s}$, and f_1^q is the unpolarized PDF. The Collins asymmetry has been measured by HERMES [3] on protons, by COMPASS on deuterons [4] and on protons [5], and at Jefferson Lab on ^{3}He [6] and found different from zero for the proton target. The Collins effect can be directly accessed in e^+e^- annihilation to hadrons, assuming that one knows the directions of the fragmenting quark and antiquark, by measuring the asymmetry [7]

$$a_{12} = \hat{a}_{\mathrm{NN}} \times \frac{\sum_q e_q^2 a^{q\uparrow\to h_1+X} D_{1q}^{h_1} \times a^{\bar{q}\uparrow\to h_2+X} D_{1\bar{q}}^{h_2}}{\sum_q e_q^2 D_{1q}^{h_1} \times D_{1\bar{q}}^{h_2}}, \quad (3)$$

where h_1 and h_2 are two back-to-back hadrons, and $\hat{a}_{\mathrm{NN}}$ is the elementary quark double transverse spin asymmetry [8]. By combining in phenomenological analyses SIDIS and e^+e^- data it has been possible to extract both the Collins FF and the transversity PDF [9–11].

It is important to have a simulation model of quark fragmentation, implemented in a Monte Carlo (MC) program, reproducing the Collins effect as well as other effects like the *dihadron asymmetry* [12–14] in the fragmentation of transversely polarized quarks and the *jet handedness* [15–17] in the fragmentation of longitudinally polarized quarks. A promising model for the polarized quark fragmentation is the recursive string + $^3P_0$ model [18–22]. This model extends the Lund model of string fragmentation [23] with the inclusion of the quark spin degree of freedom. It respects confinement, it is *left-right (LR) symmetric*[1] [23] and is based on quantum amplitudes instead of probabilities. The basic assumption which explains the spin effects is that at each string breaking the quark-antiquark pairs are produced in the $^3P_0$ state [24], namely with total spin $S = 1$, relative orbital angular momentum $L = 1$ and total angular momentum $J = 0$. Two slightly different versions of the string + $^3P_0$ model have been proposed, M18 [21] and M19 [22], the difference being the choice of an input function. Both of them are restricted to the production of pseudoscalar mesons (PS) and have been implemented in stand alone MC programs which gave similar results. In particular, they both provide a satisfactory description of the main properties of the measured Collins and dihadron asymmetries and produce also the jet-handedness effect. While M18 is more general than M19, the latter is more simple and more suitable for further developments. It has been interfaced to the hadronization part of the PYTHIA8 event generator [25] to fully exploit its predictive power and to have a more complete description of the polarized SIDIS process [26].

For a more complete description of the fragmentation process, vector meson (VM) production must be considered. Hadrons coming from VM decays in fact give an important contribution to the sample of the observed hadrons. The VM production was first included in the string + $^3P_0$ model for the process $pp^\uparrow \to \rho X$ [27] limited to the production of leading vector mesons which were treated as unpolarized. The main difficulty of including polarized VMs in the polarized quark fragmentation process is to take properly into account the spin correlations among the initial quark, the VM and the leftover quark in the recurring process $q^\uparrow \to h^\uparrow + q'^\uparrow$.

[1]*LR symmetry* should better mean *[quark] line reversal symmetry*, namely the reversal of the quark fragmentation chain.

In this paper we present the new string + $^3P_0$ model (M20), extending M19, in which the production of VMs in the polarized quark fragmentation chain is taken into account. The new model has been first presented in Ref. [28] and it is partly based on the work of Ref. [18]. It is assumed that vector mesons are coupled to quarks with coupling constants G_{L} and G_{T} for longitudinally and transversely polarized vector mesons, respectively. Besides the ratio $f_{\mathrm{VM/PS}} = |G_{\mathrm{L}}|^2 + 2|G_{\mathrm{T}}|^2$ between the abundances of vector and pseudoscalar mesons, we have essentially two new free parameters for the spin effects, $|G_{\mathrm{L}}/G_{\mathrm{T}}|$ governing the relative fraction of longitudinal and transverse vector mesons and $\theta_{\mathrm{LT}} = \arg|G_{\mathrm{L}}/G_{\mathrm{T}}|$ governing the oblique polarizations, namely the interference between longitudinal and transverse polarizations. The model is formulated at the amplitude level which automatically preserves positivity and allows to propagate the spin information along the fragmentation chain respecting quantum entanglement following the prescriptions of Refs. [29,30]. At present M20 has been implemented in a stand alone MC program which allows us to study in depth the model predictions.

The article is organized as follows. The theoretical aspects of the new model are described in Sec. II. Section III describes the stand alone MC implementation of M20. The results of the simulations including the sensitivity to the free parameters are presented in Sec. IV. New dihadron asymmetries arising from the possible oblique polarization of VMs are presented in Sec. V. The comparison with the existing SIDIS and e^+e^- data are presented in Sec. VI. The conclusions are given in Sec. VII.

II. Vector meson production in the String + $^3P_0$ model

The fragmentation process $q_A\bar{q}_B \to h_1h_2\ldots h_r\ldots h_N$, where q_A is a quark, $\bar{q}_B$ either an antiquark in e^+e^- annihilation or the target remnant in SIDIS and $h_1h_2\ldots h_r\ldots h_N$ the primary produced hadrons, is phenomenologically described as the decay of a relativistic string, stretched between q_A and $\bar{q}_B$ [23,31]. The string decay appears, in the infinite momentum frame, as a recursive series of elementary splittings $q \to h + q'$, q is the recurring splitted quark, $h = q\bar{q}'$ the emitted hadron in the splitting and q' the leftover quark. The label r indicates the rank and the rank one hadron contains q_A. We denote by k, p, and k' the four-momenta of q, h and q'. We will use the null-plane components $p^\pm = p^0 \pm p^z$ and $k^\pm = k^0 \pm k^z$. The $\hat{\mathbf{z}}$ axis or *string axis* points towards the direction of the initial quark q_A in the string rest frame. The hadron momentum can then be expressed in terms of the longitudinal splitting variable $Z = p^+/k^+$ and the hadron transverse momentum $\mathbf{p}_{\mathrm{T}} = \mathbf{k}_{\mathrm{T}} - \mathbf{k}'_{\mathrm{T}}$ with respect to the string axis, $\mathbf{k}_{\mathrm{T}}$ and $\mathbf{k}'_{\mathrm{T}}$ being the transverse momenta of q and q', respectively. The mass shell condition writes $p^+p^- = \epsilon^2$

where $\epsilon^2 = M^2 + \mathbf{p}_T^2$ is the transverse energy squared of the hadron and M its mass. The quark spin information is encoded in 2×2 density matrices $\hat{\rho}(q) = (\mathbf{1} + \boldsymbol{\sigma}\cdot\mathbf{S}_q)/2$ where $\mathbf{S}_q$ is the quark polarization vector.

The general formalism of the string $+ {}^3P_0$ model presented in Ref. [21] can include the production of mesons of arbitrary spin. The spin variable s_h of the meson enters the quark-meson-quark vertex $\Gamma_{h,s_h}(\mathbf{k}'_T, \mathbf{k}_T)$, which is a 2×2 matrix in quark spin space. s_h refers to the helicity, the spin along a chosen transverse axis or, for spin 1, specifies a linearly polarized state. To make a full Monte Carlo simulation of quark fragmentation with PS and VM production, we must add two items to the prescriptions of M18 or M19, namely

(i) the generation of M from a continuous resonant mass spectrum and
(ii) the simulation of the decay process.

The second point deserves special attention, because the spin state of the (hq') system is generally entangled. One cannot simulate separately the decay of h and the fragmentation of the leftover quark q'.

A. The $q\uparrow \to \mathrm{VM}\uparrow + q'$ splitting function

1. General formula

Let us start by including the emission of VMs in the formalism of M19 without treating the subsequent decay. To label the VM spin state, we replace s_h by the 3-vector $\mathbf{V}$, which is the space part of the covariant amplitude A^μ in the VM rest frame, as specified in Sec. II A 2. $\mathbf{V}$ is real for linear polarization, complex for vector polarization and normalized by $\mathbf{V}\cdot\mathbf{V}^* = 1$. The probability density of emitting h in the elementary splitting is given by the *splitting function*, which, when summing over the spin states of q', writes [cf. Eq. (36) of [21]]

$$F_{q',h,q}(M,\mathbf{V},Z,\mathbf{p}_T;\mathbf{k}_T,\mathbf{S}_q) \equiv \frac{dN(q\uparrow\to h\uparrow + q')}{dM^2 d^2\mathbf{p}_T dZ/Z} = \mathrm{Tr}[T(\mathfrak{q}',\mathfrak{h},\mathfrak{q})\rho(q)T^\dagger(\mathfrak{q}',\mathfrak{h},\mathfrak{q})]. \tag{4}$$

The gothic letter $\mathfrak{h} \equiv \{h, p, s_h\} = \{\text{hadron species, 4-momentum, spin state}\}$ represents the meson state, whereas $\mathfrak{q} \equiv \{q, k\} = \{\text{quark flavor, quark momentum}\}$ represents the quark state, spin excluded. T is the 2×2 *splitting matrix*, given by

$$T(\mathfrak{q}',\mathfrak{h},\mathfrak{q}) = C_{q',h,q} D_h(M)\check{g}(\epsilon^2)[(1-Z)/\epsilon^2]^{a/2} \times \exp[-b_L\epsilon^2/(2Z)]\Delta_{q'}(\mathbf{k}'_T)\Gamma_{h,\mathbf{V}}\hat{u}_q^{-1/2}(\mathbf{k}_T^2). \tag{5}$$

The coefficient $C_{q',h,q}$ is proportional to the $(\bar{q}'q)$ wave function in flavor space; a and b_L correspond to the parameters a and b of the Lund Model. $\check{g}(\epsilon^2)$ is a model input function which, like in M19, we take

$$\check{g}^2(\epsilon^2) = 1/N_a(\epsilon^2),$$
$$N_a(\epsilon^2) = \int_0^1 \frac{dZ}{Z}\left(\frac{1-Z}{\epsilon^2}\right)^a \exp(-b_L\epsilon^2/Z). \tag{6}$$

The 2×2 matrix

$$\Delta_q(\mathbf{k}_T) = (\mu + \sigma_z\boldsymbol{\sigma}\cdot\mathbf{k}_T) f_T(\mathbf{k}_T^2) \tag{7}$$

contains the spin and $\mathbf{k}_T$ dependence of the quark propagator in the string $+ {}^3P_0$ model, μ being a complex mass parameter and $f_T(\mathbf{k}_T^2)$ a fast decreasing function of $\mathbf{k}_T^2$, mainly responsible for the transverse momentum cutoff. We take $f_T(\mathbf{k}_T^2) = \exp(-b_T\mathbf{k}_T^2/2)$, with b_T a free parameter already present in the Lund model.

$D_h(M)$ has the denominator of the vector meson propagator. We take the Breit-Wigner form

$$D_h(M) = \frac{\sqrt{N_D}}{M^2 - \bar{m}_h^2 + i\bar{m}_h\gamma_h}, \tag{8}$$

where $\bar{m}_h$ is the position of the resonance peak and γ_h the resonance width, both set to the values in PDG [32]. N_D is the normalization constant of the mass distribution $|D_h(M)|^2$ of the resonance.

The 2×2 matrix $\Gamma_{h,\mathbf{V}}$ sets the coupling of the vector meson to the quark line. Its most simple form is [18]

$$\Gamma_{h,\mathbf{V}} = G_T\boldsymbol{\sigma}_T\cdot\mathbf{V}_T^*\sigma_z + G_L V_z^*\times\mathbf{1}. \tag{9}$$

G_L and G_T are the coupling constants for longitudinal and transverse linear polarizations of the VM. This decomposition is analogous to that in G_M and G_E of the nucleon form factor and that in ${}^3S_1$ and ${}^3D_1$ of the deuteron wave function. In a covariant quark-multiperipheral model the analog couplings would be γ^μ and $\sigma^{\mu\nu}p_\nu$. We allow G_L/G_T to be complex, as a result of different quantum actions of the initial string for the L and T polarizations. In the following we will use as parameters

$$|G_L/G_T|, \qquad \theta_{LT} = \arg(G_L/G_T), \tag{10}$$

which are the new free parameters of M20. A relevant quantity is the fraction

$$f_L = \frac{|G_L|^2}{2|G_T|^2 + |G_L|^2}; \tag{11}$$

for $\mathbf{S}_q = \mathbf{0}$ it is $f_L = \hat{\rho}_{ll}$ [see Eq. (33)], hence f_L is the fraction of the longitudinally polarized vector mesons.

$\hat{u}_q$ is a 2×2 matrix given by Eq. (47) of [21], which we decompose as

$$\hat{u}_q(\mathbf{k}_\mathrm{T}) = \sum_h \hat{u}_{q,h}(\mathbf{k}_\mathrm{T}), \tag{12}$$

$$\hat{u}_{q,h}(\mathbf{k}_\mathrm{T}) = |C_{q',h,q}|^2 \int d^2\mathbf{k}'_\mathrm{T} \breve{g}^2(\epsilon^2) N_a(\epsilon^2) \times \sum_{s_h} \Gamma^\dagger_{h,s_h} \Delta^\dagger_{q'}(\mathbf{k}'_\mathrm{T}) \Delta_{q'}(\mathbf{k}'_\mathrm{T}) \Gamma_{h,s_h}. \tag{13}$$

$\hat{u}_{q,h}(\mathbf{k}_\mathrm{T})$ is the contribution of hadron species h. For vector mesons, $s_h = \mathbf{V}$ and $\sum_\mathbf{V}$ is made over three orthonormal basic vectors.[2] For pseudoscalar mesons it is $s_h \equiv 0$ and $\Gamma_h = \sigma_z$.

With our choice $\breve{g}^2(\epsilon^2) N_a(\epsilon^2) = 1$ (choice of M19) both $\hat{u}_q(\mathbf{k}_\mathrm{T})$ and $\hat{u}_{q,h}(\mathbf{k}_\mathrm{T})$ become proportional to the unit matrix and independent of $\mathbf{k}_\mathrm{T}$:

$$\hat{u}_{q,h} = \mathbf{1} \times |C_{q',h,q}|^2 (|\mu|^2 + \langle \mathbf{k}^2_\mathrm{T} \rangle_{f_\mathrm{T}}) \times \begin{cases} 1 & \text{(PS case)} \\ (2|G_\mathrm{T}|^2 + |G_\mathrm{L}|^2) & \text{(VM case)} \end{cases}, \tag{14}$$

with the notation

$$\langle \mathbf{k}^2_\mathrm{T} \rangle_{f_\mathrm{T}} \equiv \int d^2\mathbf{k}_\mathrm{T} \mathbf{k}^2_\mathrm{T} f^2_\mathrm{T}(\mathbf{k}^2_\mathrm{T}) / \int d^2\mathbf{k}_\mathrm{T} f^2_\mathrm{T}(\mathbf{k}^2_\mathrm{T}), \tag{15}$$

where f_T is the function appearing in Eq. (7). So, from now $\hat{u}_q(\mathbf{k}^2_\mathrm{T})$ and $\hat{u}_{q,h}(\mathbf{k}^2_\mathrm{T})$ will be considered as constant numbers and we will omit "$\mathbf{1}\times$" which appears in Eq. (14). The relative probability of getting the hadron species h in the splitting $q \to h + q'$ is then

$$P(q \to h + q') = \hat{u}_{q,h}/\hat{u}_q. \tag{16}$$

It is independent of $\mathbf{k}_\mathrm{T}$ and of the polarization of q, contrary to other choices of the function $\breve{g}(\epsilon^2)$.

2. Frame for the polarization vector V

$\mathbf{V}$ is obtained from the covariant 4-vector A^μ of the VM wave function by bringing the VM at rest via two successive Lorentz boosts: a longitudinal one B_L^{-1} which suppresses p_z and a transverse one B_T^{-1} which suppresses $\mathbf{p}_\mathrm{T}$, where

$$B_\mathrm{T} = B(\mathbf{p}_\mathrm{T}/\epsilon), \qquad B_\mathrm{L} = B(p_z \hat{\mathbf{z}}/E) \tag{17}$$

and the argument of B is the velocity vector of the boost. The action of B_T and B_L is shown in Fig. 1. Thus $(0, \mathbf{V}) = B_\mathrm{T}^{-1} B_\mathrm{L}^{-1} A^\mu$. This transformation preserves the longitudinal Lorentz invariance and the LR symmetry [23] of the model. We call *LR symmetric (rest) frame* the resulting reference frame for $\mathbf{V}$ (also named *PL frame* in Ref. [33]).

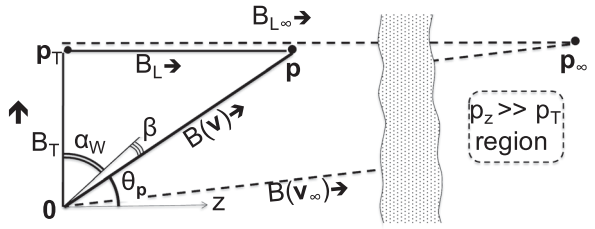

FIG. 1. Boost compositions involved in the definition of $\mathbf{V}$ and the Wigner angle α_W, following Eqs. (17) and (18). $\mathbf{v} = \mathbf{p}/E$. The dashed lines figure the $p_z \to \infty$ limit, Eq. (20).

The VM could have been put at rest with the direct boost $B^{-1}(\mathbf{p}/E)$, leading to a different vector $\mathbf{V}_\mathrm{hl}$ ("hl" refers to the so-called *helicity frame*). We have $(0, \mathbf{V}) = \mathcal{R}_\mathrm{W}(0, \mathbf{V}_\mathrm{hl})$ where $\mathcal{R}_\mathrm{W} = B_\mathrm{T}^{-1} B_\mathrm{L}^{-1} B(\mathbf{p}/E)$ is a *Wigner rotation* about $\hat{\mathbf{z}} \times \mathbf{p}$, of angle $\alpha_\mathrm{W}(\mathbf{p}/E)$ given by

$$\alpha_\mathrm{W}(\mathbf{p}/E) = \arcsin\left(\frac{p_z p_\mathrm{T}}{E\epsilon + M\epsilon}\right), \quad = \frac{\pi}{2} - \theta_\mathbf{p} - \beta; \quad \beta = \arcsin\left(\frac{M p_z}{\epsilon |\mathbf{p}|}\right) \tag{18}$$

and represented in Fig. 1.[3] $\mathbf{V}_\mathrm{hl}$ and $\alpha_\mathrm{W}(\mathbf{p}/E)$ are not invariant under a longitudinal boost. In particular, in the SIDIS process they change from the target frame to the γ^*-nucleon frame. When $p_z \to +\infty$ (dashed lines of Fig. 1) the helicity frame becomes the *null plane (rest) frame* and

$$\mathbf{V}_\mathrm{hl} \to \mathbf{V}_\mathrm{npl}. \tag{19}$$

$$\alpha_\mathrm{W}(\mathbf{p}/E) \to \alpha_{\mathrm{W}\infty} = \arctan(p_\mathrm{T}/M). \tag{20}$$

$\mathbf{V}_\mathrm{npl}$ is longitudinally Lorentz invariant but not LR symmetric.

The above transformations also serve to adjust the individual momenta $\mathbf{p}^*_1, \mathbf{p}^*_2, \ldots$ or the relative momenta of the decay products in the rest frame of the VM. For a 2-body decay, the relative 4-momentum $p^\mu_\mathrm{rel} = (E^*_2 p^\mu_1 - E^*_1 p^\mu_2)/M$ [with $E^*_i = P \cdot p_i / M$ and $M^2 = P^2 \equiv (p_1 + p_2)^2$] transforms like A^μ;

$$\mathbf{r} \equiv \mathbf{p}^*_\mathrm{rel} = \mathbf{p}^*_1 = -\mathbf{p}^*_2 \tag{21}$$

is the analog of $\mathbf{V}$ and

[2]Due to the fluctuating mass of the VM, one should insert $\int dM^2 |D_h(M)|^2$ in Eq. (13) before the integral over $\mathbf{k}'_\mathrm{T}$.

[3]Other expressions are $\alpha_\mathrm{W} = \mathbf{N} \cdot \int_C (\mathbf{p} \times d\mathbf{p})/(E^2 + mE) = M \int \int_A d^2\mathbf{p}/E^3$, where C is the closed path run by the vector $\mathbf{p}$ in the successive boosts $B(\mathbf{p}/E)$, B_L^{-1}, B_T^{-1}, and A is the area enclosed by C, and $\mathbf{N}$ is defined in Eq. (23).

$$\mathbf{R} = \begin{pmatrix} \mathbf{R}_T \\ R_z \end{pmatrix} = \frac{1}{z_1 + z_2} \begin{pmatrix} z_2 \mathbf{p}_{1T} - z_1 \mathbf{p}_{2T} \\ E_2^* z_1 - E_1^* z_2 \end{pmatrix} \quad (22)$$

is the analog of $\mathbf{V}_{npl}$. $\mathbf{R}$ is obtained from $\mathbf{r}$ in the LR symmetric frame by the rotation of angle $-\alpha_{W\infty}$ about $\hat{\mathbf{z}} \times \mathbf{p}_T$. $\mathbf{R}_T$ is the relative transverse momentum involved in the dihadron asymmetry, whether or not h_1 and h_2 come from a resonance. It was introduced and named $\boldsymbol{\kappa}_\tau$ in Ref. [34].

3. Coordinates in the rest frame

Independently of the choice of frame (LR symmetric or null plane) we need three basic vectors to define the coordinates of $\mathbf{S}_q$, $\mathbf{V}$, $\mathbf{p}_1^*$, or $\mathbf{R}$. A natural basis, $\{\mathbf{L}, \mathbf{M}, \mathbf{N}\}$, is linked to the meson transverse momentum $\mathbf{p}_T$:

$$\mathbf{L} = \hat{\mathbf{z}}, \qquad \mathbf{M} = \mathbf{p}_T/|\mathbf{p}_T|, \qquad \mathbf{N} = \hat{\mathbf{z}} \times \mathbf{M}. \quad (23)$$

We will also use the $\{\mathbf{l}, \mathbf{m}, \mathbf{n}\}$ basis linked to the antiquark momentum $-\mathbf{k}'_T$,

$$\mathbf{l} = \hat{\mathbf{z}}, \qquad \mathbf{m} = -\mathbf{k}'_T/|\mathbf{k}'_T|, \qquad \mathbf{n} = \hat{\mathbf{z}} \times \mathbf{m}, \quad (24)$$

and the $\{\mathbf{X}, \mathbf{Y}, \mathbf{Z}\}$ basis linked to the quark transverse polarization,

$$\mathbf{Y} = \mathbf{S}_{qT}/|\mathbf{S}_{qT}|, \qquad \mathbf{Z} = \hat{\mathbf{z}}, \qquad \mathbf{X} = \mathbf{Y} \times \mathbf{Z}. \quad (25)$$

These bases are simply related by rotations about $\hat{\mathbf{z}}$. From now on, $\mathbf{S}_q$, $\mathbf{S}_q \cdot \mathbf{n}$, $\mathbf{S}_q \cdot \mathbf{X}$ etc., will shortly be written $\mathbf{S}$, S_n, S_X etc. To a vector $\mathbf{V}$ is associated the pure spin state of the vector meson

$$\begin{aligned} |\mathbf{V}\rangle &= V_L|\mathbf{L}\rangle + V_M|\mathbf{M}\rangle + V_N|\mathbf{N}\rangle, \\ &= V_l|\mathbf{l}\rangle + V_m|\mathbf{m}\rangle + V_n|\mathbf{n}\rangle, \text{etc.} \end{aligned} \quad (26)$$

Note that $|\mathbf{V}\rangle$ and $|-\mathbf{V}\rangle$ are the same state.

4. Splitting function for pseudoscalar mesons

Before studying the splitting function for vector mesons, let us first recall the one for pseudoscalar mesons [cf. Eq. (26) of [22]]. Removing the argument $\mathbf{V}$ in Eq. (4) and using Eqs. (5)–(7) and (9)–(16), one gets

$$\begin{aligned} &F_{q',h(\mathrm{PS}),q}(Z, \mathbf{p}_T; \mathbf{k}_T, \mathbf{S}_q) \\ &= \frac{\hat{u}_{q,h}}{\hat{u}_q} \frac{f_1^2(\mathbf{k}_T'^2)}{|\mu|^2 + \langle \mathbf{k}_T^2 \rangle_{f_T}} N_a^{-1}(\epsilon^2) \left(\frac{1-Z}{\epsilon^2}\right)^a \exp\left(-b_L \epsilon^2/Z\right) \\ &\quad \times (|\mu|^2 + \mathbf{k}_T'^2)[1 + \hat{a} S_n], \end{aligned} \quad (27)$$

with

$$\hat{a} \equiv \frac{2\mathrm{Im}(\mu) k'_T}{|\mu|^2 + \mathbf{k}_T'^2} > 0. \quad (28)$$

The square bracket of Eq. (27) is responsible for the Collins effect, since $\mathbf{n}$ is correlated with $\mathbf{N}$. In particular, $\mathbf{n} = \mathbf{N}$ for a rank one hadron.

5. Splitting function for vector mesons

In the case of vector mesons, selecting one polarization of the $\{\mathbf{l}, \mathbf{m}, \mathbf{n}\}$ basis, we obtain from Eqs. (4)–(7), Eqs. (9)–(16), and Eq. (28)

$$\begin{aligned} &F_{q',h,q}(M, \mathbf{V}, Z, \mathbf{p}_T, \mathbf{k}_T, \mathbf{S}_q) \\ &= \frac{\hat{u}_{q,h}}{\hat{u}_q} |D_h(M)|^2 f_1^2(\mathbf{k}_T'^2) \frac{(|\mu|^2 + \mathbf{k}_T'^2)}{|\mu|^2 + \langle \mathbf{k}_T^2 \rangle_{f_T}} \\ &\quad \times N_a^{-1}(\epsilon^2) \left(\frac{1-Z}{\epsilon^2}\right)^a \exp\left(-b_L \epsilon^2/Z\right) \\ &\quad \times \begin{cases} (1 - \hat{a} S_n) f_L & \text{for } \mathbf{V} = \mathbf{l} \\ (1 - \hat{a} S_n)(1 - f_L)/2 & \text{for } \mathbf{V} = \mathbf{m} \\ (1 + \hat{a} S_n)(1 - f_L)/2 & \text{for } \mathbf{V} = \mathbf{n} \\ 1 - f_L \hat{a} S_n & \text{for the sum over } \mathbf{V} \end{cases}. \end{aligned} \quad (29)$$

The last line after the brace is for the case where the VM polarization is not analyzed. Equation (29) with this choice and Eq. (27) are used in simulations to generate first the vector or pseudoscalar meson species of the emitted particle, then its transverse momentum $\mathbf{p}_T = \mathbf{k}_T - \mathbf{k}'_T$ and then its Z.

Global Collins effect.—It is the Collins effect of the vector meson and it comes from the S_n term of Eq. (29). It is to be distinguished from the dihadron asymmetry (or relative Collins effect) of the decay products. These have individual Collins effects resulting from both the global and the relative one.

For a rank one meson, $-\mathbf{k}'_T = \mathbf{p}_T$ and $\mathbf{n} = \mathbf{N}$. Then the analyzing power $a^{q_A\uparrow \to h+X}(z, p_T)$ is equal to the coefficient of S_n in Eq. (27) for PS mesons or (29) for VM. It is maximum for $|\mathbf{p}_T| = |\mu|$. For the VM, it depends on the linear polarization, as pictured in Fig. 2, which gives a semiclassical description of PS and VM production in the model. If the VM polarization is normal to the production plane as in Fig. 2(a), then the Collins asymmetry equals that of a pion of the same $|\mathbf{p}_T|$. If the polarization is in the production plane as in Fig. 2(b), then the asymmetry is opposite to that of a pion.

A "hidden spin" effect.—Figure 3 is the analog of Fig. 2 for a meson of rank ≥ 2. It shows that the quark and the antiquark transverse momenta are on the same side for a PS meson [Fig. 3(a)]. The same occurs for a VM with probability $(1 - f_L)/2$. In the case of Fig. 3(b), which occurs with probability $(1 + f_L)/2$, the q and $\bar{q}'$ momenta are on the opposite sides. So, $\langle \mathbf{p}_T{}^2 \rangle$ is expected to be larger for PS mesons than for VMs. This prediction is

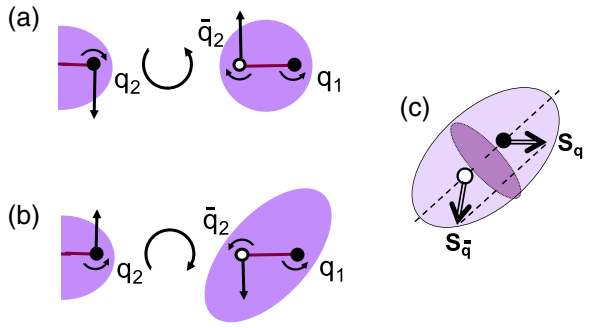

FIG. 2. Production mechanism of a first-rank meson in the string $+{}^3P_0$ model. (a) PS meson or VM of linear polarization perpendicular to the figure plane (the $\hat{\mathbf{z}}$, $\mathbf{p}_T$ plane). (b) VM of linear polarization in this plane. Straight simple arrows represent quark or antiquark momenta. Circular arrows represent quark spins or $q\bar{q}$ relative orbital momenta. Linearly polarized VMs are represented by ellipsoids. (c) Correlations between the ellipsoid major axis, the q spin and the $\bar{q}$ spin.

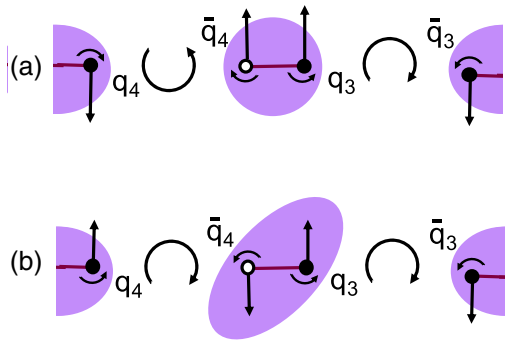

FIG. 3. Production mechanism of a rank ≥ 2 meson, here the $q_3\bar{q}_4$ meson. Same notations as in Fig. 2.

independent on the polarization of the initial quark and specific of the ${}^3P_0$ mechanism. It could be tested in unpolarized experiments, looking at "unfavored" quark fragmentation or at the central rapidity region.

B. The density matrix of the vector meson

Rewriting $T(\mathfrak{q}', \mathfrak{h}, \mathfrak{q})$, defined in Eq. (5), as $T_\alpha(\mathfrak{q}', \mathfrak{h}, \mathfrak{q})V_\alpha$, the relative probability to find the VM in a state $|\mathbf{V}\rangle$ is of the form

$$\langle \mathbf{V}|\hat{\rho}(h)|\mathbf{V}\rangle = V^*_\alpha \hat{\rho}_{\alpha\alpha'}(h) V_{\alpha'} \tag{30}$$

where α and $\alpha' \in \{L, M, N\}$ or $\{l, m, n\}$ or $\{X, Y, Z\}$, depending on the basis, and

$$\hat{\rho}_{\alpha\alpha'}(h) = \frac{\mathrm{Tr}\{T_\alpha \hat{\rho}(q) T^\dagger_{\alpha'}\}}{\sum_\beta \mathrm{Tr}\{T_\beta \hat{\rho}(q) T^\dagger_\beta\}}, \\ = \frac{\mathrm{Tr}\{(\mu + \sigma_z \boldsymbol{\sigma}\cdot\mathbf{k}'_T)\Gamma_{h,\alpha}\hat{\rho}(q)\Gamma^\dagger_{h,\alpha'}(\mu^* + \boldsymbol{\sigma}\cdot\mathbf{k}'_T\sigma_z)\}}{(|\mu|^2 + \mathbf{k}'^2_T)N(\mathbf{S})}, \tag{31}$$

with

$$N(\mathbf{S}) = 2|G_T|^2 + |G_L|^2 - |G_L|^2 \hat{a} S_n. \tag{32}$$

$\hat{\rho}_{\alpha\alpha'}(h)$ is the polarization matrix or *(spin) density matrix* of the VM, normalized to $\mathrm{Tr}\hat{\rho}(h) = 1$.

The real part of $\hat{\rho}$ is the *tensor*, or *linear* polarization.[4] It is convenient to represent it by a *polarization ellipsoid* as in Figs. 2–5. The axes of this ellipsoid are parallel to the eigenvectors of $\mathrm{Re}\hat{\rho}$ and their half-lengths are equal to the square roots of the eigenvalues (see Appendix A). $\mathrm{Re}\hat{\rho}$ governs the angular distribution of the decay product. Thus, in the VM $\to h_1 h_2$ decay, the relative $h_1 h_2$ momentum tends to be aligned with the major axis (but without preferred sense).

In the $(\mathbf{l}, \mathbf{m}, \mathbf{n})$ basis $\mathrm{Re}\hat{\rho}_{\alpha\alpha'}(h)$ writes the following:

$$\begin{aligned}
\hat{\rho}_{\mathrm{ll}} &= (1 - \hat{a}S_n)|G_L|^2/N(\mathbf{S}), \\
\hat{\rho}_{\mathrm{mm}} &= (1 - \hat{a}S_n)|G_T|^2/N(\mathbf{S}), \\
\hat{\rho}_{\mathrm{nn}} &= (1 + \hat{a}S_n)|G_T|^2/N(\mathbf{S}), \\
\mathrm{Re}\hat{\rho}_{\mathrm{mn}} &= \hat{a}S_m|G_T|^2/N(\mathbf{S}), \\
\mathrm{Re}\hat{\rho}_{\mathrm{ml}} &= (\hat{a} - S_n)\sin\theta_{LT}|G_L G_T|/N(\mathbf{S}), \\
\mathrm{Re}\hat{\rho}_{\mathrm{nl}} &= (\hat{a}\cos\theta_{LT}S_l - \sin\theta_{LT}S_m)|G_L G_T|/N(\mathbf{S}),
\end{aligned} \tag{33}$$

together with $\mathrm{Re}\hat{\rho}_{\alpha\alpha'} = \mathrm{Re}\hat{\rho}_{\alpha'\alpha}$.[5] These are in accordance with Eq. (29) and satisfy automatically the positivity conditions.

The imaginary, antisymmetric part of $\hat{\rho}(h)$ is the *vector* or *circular* polarization. It plays no role in the decay processes considered here. The complete matrix elements are given in Appendix A.

Aligned and transverse linear polarizations.—The element $\hat{\rho}_{\mathrm{ll}} \equiv \hat{\rho}_{\mathrm{LL}}$ is related to the *alignment* parameter $(3\hat{\rho}_{\mathrm{LL}} - 1)/2$. The elements $\hat{\rho}_{\mathrm{mm}}$, $\hat{\rho}_{\mathrm{nn}}$, and $\hat{\rho}_{\mathrm{mn}}$ define the transverse linear polarization, whereas $\hat{\rho}_{\mathrm{ml}}$ and $\hat{\rho}_{\mathrm{nl}}$ depend on θ_{LT} and describe *oblique* polarizations. Note, however, that our separation in *aligned*, *transverse* and *oblique* is linked to our choice of the Lorentz transformations bringing the meson at rest.

Figure 4 represents, for a first-rank VM and various orientations of $\mathbf{p}_T$ with respect to $\mathbf{S}_T$, the transverse linear polarization defined by the 2×2 restricted matrix $\mathrm{Re}\hat{\rho}^{(T)}_{\alpha\alpha'} = \mathrm{Re}\hat{\rho}_{\alpha\alpha'}$ for α and $\alpha' \neq z$. The ellipses are the projections of the polarization ellipsoids. Their axes are parallel to the eigenvectors of $\hat{\rho}^{(T)}$ and have lengths equal to the square roots of the eigenvalues $(1 \pm \hat{a}|\mathbf{S}_T|)|G_T|^2/N(\mathbf{S})$ of $\hat{\rho}^{(T)}$. Note that for a 2-body decay and $\phi(\mathbf{p}_T) = \pi$ (case of ellipse E_2), the left-moving decay hadron gets a large transverse momentum and the same Collins effect as the VM itself.

[4] A general description of the density matrix for spin 1 particles can be found in Ref. [35].

[5] Equation (27) of [18] is in agreement with Eq. (33) except for its wrong sign in front of $2\mathrm{Im}(\mu)(\mathbf{V}_T \cdot \tilde{\mathbf{t}}\mathbf{V}_T \cdot \mathbf{S} + \mathbf{V}_T \cdot \mathbf{t}\mathbf{V}_T \cdot \tilde{\mathbf{S}})$.

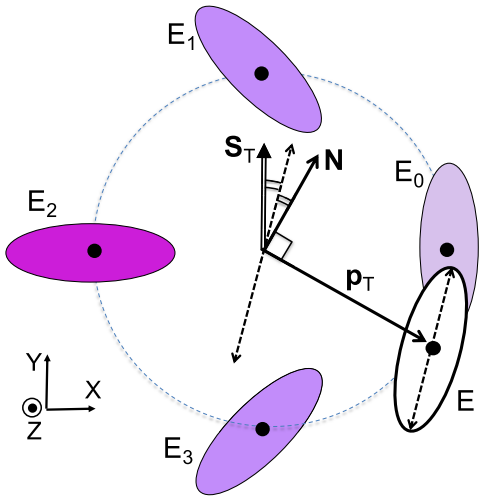

FIG. 4. Transverse polarization of a first-rank vector meson, for azimuths $\phi(\mathbf{p}_T) = j\pi/2$ $(j = 0, \ldots 3)$ of $\mathbf{p}_T$ in the $(\mathbf{X}, \mathbf{Y})$ frame. The ellipses are projections of the polarization ellipsoids. The darknesses of E_j figure the depths $\propto (\hat{\rho}_{ZZ})^{1/2}$ of the ellipsoids in the Z direction. Ellipse E is for an ordinary azimuth. Its major axis (dashed) is parallel to the bisector of $\mathbf{S}_T$ and $\mathbf{N}$.

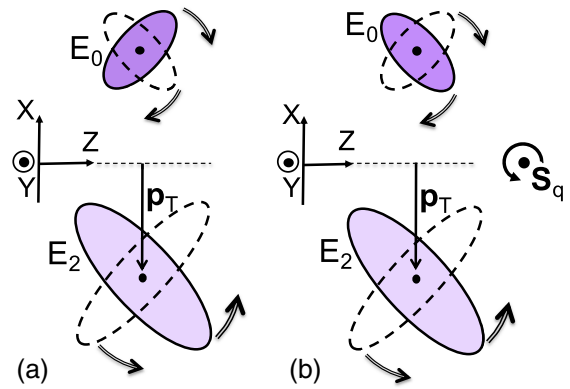

FIG. 5. Oblique polarization in the $(\mathbf{Z}, \mathbf{X})$ plane of a first-rank vector meson, corresponding to cases E_0 and E_2 of Fig. 4. (a) with only the $\hat{a}\sin\theta_{LT}$ term in $\mathrm{Re}\hat{\rho}_{ml}$ in Eq. (33). (b) with only the $\sin\theta_{LT}S_Y$ term in $\mathrm{Re}\hat{\rho}_{XZ}$ in Eq. (B2). The continuous (dashed) contours are for positive (negative) $S_Y \sin\theta_{LT}$. Ellipsoid E_0 is drawn darker to figure its larger depth $\propto (\rho_{YY})^{1/2}$ in the Y direction. The bent arrows indicate the Wigner rotation when passing from the LR symmetric to the null-plane frame, according to Eqs. (19) and (20).

Oblique polarizations.—They are interferences between transverse and longitudinal amplitudes, therefore depend on $|G_L G_T|$ and θ_{LT} and correspond to the elements $\hat{\rho}_{ml}$ and $\hat{\rho}_{nl}$. We analyze it in the basis $\{\mathbf{X}, \mathbf{Y}, \mathbf{Z}\}$ introduced in Eq. (25). Let us consider separately, in Eq. (33) or (B2), the effects of the terms $\hat{a}\sin\theta_{LT}$, $\hat{a}\cos\theta_{LT}S_z$, and $\sin\theta_{LT}\mathbf{S}_T$ in $\hat{\rho}_{ml}$ and $\hat{\rho}_{nl}$.

The term $\hat{a}\sin\theta_{LT}$ in $\hat{\rho}_{ml}$ is independent of the quark polarization and gives an oblique polarization in the $\mathbf{l}$, $\mathbf{m}$ plane, projected on the $(\mathbf{X}, \mathbf{Z})$ plane in Fig. 5(a). For the 2-body decay VM $\to h_1 h_2$ it acts upon the dependence of $\langle \mathbf{p}_{Ti}^2 \rangle$ on z_i: at large z_1, p_{1z}^* is likely positive and, for rank one, Fig. 5(a) indicates a larger $\langle \mathbf{p}_{1T}^2 \rangle$ for positive than for negative $\sin\theta_{LT}$. It comes from the $\mathbf{p}_T$ composition law

$$\mathbf{p}_{iT} = \mathbf{p}_{iT}^* + [E_i^* + \mathbf{p}_T \cdot \mathbf{p}_{iT}^*(\epsilon + M)]\mathbf{p}_T/M \qquad (34)$$

and the fact that the sign of $\mathbf{p}_T \cdot \mathbf{p}_{iT}^*$ is most likely that of $p_{iz}^* \times \sin\theta_{LT}$. The term $\hat{a}\cos\theta_{LT}S_l$ in $\hat{\rho}_{nl}$ gives an oblique polarization in the $(\mathbf{l}, \mathbf{n})$ plane. This is a *jet handedness* effect like the one with only direct pions treated in Sec. VI of [21]. For the decay of a first-rank VM in two mesons h_1, h_2 we have at fixed $\mathbf{p}_{1z}^*$

$$\mathbf{p}_{1z}^* \langle (\mathbf{p}_1 \times \mathbf{p}_2)_z \rangle = -(2/5)\mathrm{Re}\hat{\rho}_{nl}|\mathbf{p}_1^*|^2|\mathbf{p}_T|. \qquad (35)$$

The terms in $\sin\theta_{LT}\mathbf{S}_T$, gathered in one term of (B2), are independent of $\mathrm{Im}\mu$ and produce an oblique polarization in the $(\mathbf{X}, \mathbf{Z})$ plane [Fig. 5(b)]. In a 2-body decay it contributes to the individual Collins asymmetry of the decay products. Considering Eq. (34), we see that at fixed z_i this obliquity adds to or subtracts from the part inherited from the global Collins effect. This effect will be studied in more detail in Sec. IV C 2.

The oblique polarization is also a source of dihadron asymmetry, which bears on the variable $\mathbf{R}_T$ defined in Eq. (22). The asymmetry sign is not simply deduced from the orientation of the ellipses in Fig. 5, due to the Wigner rotation. In Eq. (22) the distinction between h_1 and h_2 must not be done according to their charges (like $h_1 = \pi^+$, $h_2 = \pi^-$) but between "fast" and "slow," for instance, by $z_1 > z_2$. A distinction by the charges gives no dihadron asymmetry because of the $\mathbf{p}_1^* \leftrightarrow \mathbf{p}_2^*$ invariance of the decay angular distribution. This dihadron asymmetry is not the result of an interference with a nonresonant amplitude. It is related to the fragmentation function $H_{1\,LT}$ of Ref. [36]. The asymmetry will be discussed in more detail in Sec. V.

C. The decay of a polarized VM

Decay in two pseudoscalar mesons.—We suppose that, by the Monte Carlo method, we have generated the species h of the VM, its running mass M, its momentum $\mathbf{p}$ and calculated its density matrix $\hat{\rho}_{\alpha\alpha'}$ in the $\{\mathbf{l}, \mathbf{m}, \mathbf{n}\}$ basis, for instance, with Eq. (33).

First, one chooses the h_1 and h_2 species, e.g., $K^+\pi^0$ for a K^{*+}, following the known branching ratio. This fixes the modulus of the relative momentum $\mathbf{r} = \mathbf{p}_1^* = -\mathbf{p}_2^*$ in the VM rest frame,

$$|\mathbf{r}| = (2M)^{-1}[M^2 - m_+^2]^{1/2} \times [M^2 - m_-^2]^{1/2}, \qquad (36)$$

where $m_\pm = m_1 \pm m_2$. It remains to generate its direction $\hat{\mathbf{r}}$. The decay amplitude is

$$\mathcal{M}(\mathrm{VM} \to h_1 h_2) = g_{hh_1h_2} A^\mu (p_1 - p_2)_\mu = -2 g_{hh_1h_2} \mathbf{V}\cdot\mathbf{r}. \tag{37}$$

Then, the resonant $q \to h_1 + h_2 + q'$ amplitude is proportional to

$$\sum_{\mathbf{V}=\mathbf{l},\mathbf{m},\mathbf{n}} T_\alpha V_\alpha V_\beta r_\beta = T_\alpha r_\alpha, \tag{38}$$

and the angular distribution takes the form

$$d\mathcal{N}(\hat{\mathbf{r}})/d\Omega = 3(4\pi)^{-1} \hat{r}_\alpha \hat{\rho}_{\alpha\alpha'}(h) \hat{r}_{\alpha'}, \tag{39}$$

reminiscent of Eq. (30). A corresponding formula is found in Eq. (B10) of Ref. [36].

Decay $\omega \to \pi^0\gamma$.—The decay amplitude is

$$\mathcal{M}(\omega \to \pi^0\gamma) \propto \mathbf{V}_\omega \cdot (\mathbf{V}_\gamma \times \mathbf{r}), \tag{40}$$

where $\mathbf{V}_\gamma \perp \mathbf{r}$ is the vector amplitude of the photon and $\mathbf{r} = \mathbf{p}^*_\gamma$. Averaging over $\mathbf{V}_\gamma$, we have to replace in Eq. (39) $\hat{r}_\alpha \hat{r}_{\alpha'}$ by the tensor $(1/2)(\delta_{\alpha\alpha'} - \hat{\mathbf{r}}_\alpha \hat{\mathbf{r}}_{\alpha'})$.

Decay ω or $\phi \to \pi^+\pi^-\pi^0$.—Due to parity conservation the invariant decay amplitude in three pseudoscalars is of the form

$$\mathcal{M}(\mathrm{VM} \to h_1 h_2 h_3) \propto \mathcal{F}(s_1, s_2, s_3) \mathbf{V}\cdot\boldsymbol{\tau}, \tag{41}$$

where $\boldsymbol{\tau} = \mathbf{p}^*_1 \times \mathbf{p}^*_2$ is normal to the *decay plane*, $s_i = (p_j + p_k)^2$ and $\{i, j, k\}$ is a cyclic permutations of $\{1, 2, 3\}$. From energy-momentum conservation, $\mathbf{p}^*_1 + \mathbf{p}^*_2 + \mathbf{p}^*_3 = \mathbf{0}$ and $E^*_1 + E^*_2 + E^*_3 = M$, which is the variable mass of the resonance. The E^*_i are linearly related to the s_i by

$$E^*_i = [\mathbf{p}^{*}_i + m_i^2]^{1/2} = (M^2 + m_i^2 - s_i)/(2M). \tag{42}$$

Taking into account energy-momentum conservation, the 3-body phase space element reduces to

$$d\Phi(\mathbf{p}^*_1, \mathbf{p}^*_2) \propto d\Omega(\boldsymbol{\tau}) d\phi_{1|\boldsymbol{\tau}} dE^*_1 dE^*_2, \tag{43}$$

where $\phi_{1|\boldsymbol{\tau}}$ is the azimuth of $\mathbf{p}^*_1$ about $\boldsymbol{\tau}$. In the (E^*_1, E^*_2) plane (Dalitz plot) the physical phase space is limited to the domain

$$\boldsymbol{\tau}^2 \equiv \mathbf{p}^{*2}_1 \mathbf{p}^{*2}_2 - (1/4)(\mathbf{p}^{*2}_1 + \mathbf{p}^{*2}_2 - \mathbf{p}^{*2}_3)^2 \geq 0. \tag{44}$$

The *form factor* $\mathcal{F}(s_1, s_2, s_3)$ depends on the dynamics, in particular on final state 2-body interactions. Following the isobar model, we assume that the VM decay occurs in two steps, $h \to \pi^i + \bar{\rho}^i$, then $\bar{\rho}^i \to \pi^j + \pi^k$, where now $\{+, 0, -\}$ replace $\{1, 2, 3\}$. So, we take

$$\mathcal{F}(s_+, s_-, s_0) = \sum_{i=+,0,-} \frac{g_{h\bar{\rho}^i\pi^i} g_{\bar{\rho}^i\pi^j\pi^k}}{s_i - \bar{m}^2_{\rho^i} + i\bar{m}_{\rho^i}\hat{\gamma}_{\rho^i}}. \tag{45}$$

By isospin symmetry the coupling constants $g_{h\rho\pi}$ and $g_{\rho\pi\pi}$ do not depend on the charge of the intermediate ρ meson: $g_{h\rho^+\pi^-} = g_{h\rho^-\pi^+} = g_{h\rho^0\pi^0}$ and $g_{\rho^+\pi^0\pi^+} = g_{\rho^-\pi^-\pi^0} = g_{\rho^0\pi^+\pi^-}$.

To generate the pion momenta $\mathbf{p}^*_i$, we proceed in three steps. First we draw E^*_1 and E^*_2 according to the (not normalized) distribution

$$w(E^*_1, E^*_2) = \boldsymbol{\tau}^2 |\mathcal{F}(s_1, s_2, s_3)|^2. \tag{46}$$

and calculate $|\mathbf{p}_1|$, $\mathbf{p}_1 \cdot \mathbf{p}_2$, and $|\boldsymbol{\tau}|$.

Then we generate $\hat{\boldsymbol{\tau}} = \boldsymbol{\tau}/|\boldsymbol{\tau}|$ according to Eq. (39) with $\hat{\mathbf{r}} \to \hat{\boldsymbol{\tau}}$. Indeed, $\hat{\boldsymbol{\tau}}$ plays the same role as $\hat{\mathbf{r}}$ in the two-body decay.

Then we draw at random $\phi_{1|\boldsymbol{\tau}}$ in $[0, 2\pi]$ and build

$$\mathbf{p}^*_1 = |\mathbf{p}^*_1| \mathcal{R}_{\hat{\mathbf{z}}\times\boldsymbol{\tau}}(\theta^*_{\boldsymbol{\tau}}) (\cos\phi_{1|\boldsymbol{\tau}}, \sin\phi_{1|\boldsymbol{\tau}}, 0)^{\mathrm{T}}, \tag{47}$$

where $\theta^*_{\boldsymbol{\tau}}$ is the polar angle of $\boldsymbol{\tau}$.

Finally we build $\mathbf{p}^*_2$ and $\mathbf{p}^*_3 = -\mathbf{p}^*_1 - \mathbf{p}^*_2$, using

$$\mathbf{p}^*_2 = |\mathbf{p}^*_1|^{-2} [(\mathbf{p}_1 \cdot \mathbf{p}_2)\mathbf{p}^*_1 + \boldsymbol{\tau} \times \mathbf{p}^*_1]. \tag{48}$$

Boosting the decay mesons.—Once $(E^*_i, \mathbf{p}^*_i)$ have been generated, the momenta $(E_i, \mathbf{p}_i)$ in the string frame are obtained by the inverse of the boosts which serve to define $\mathbf{V}$ in Sec. II A 2:

$$(E_i, \mathbf{p}_i) = B_{\mathrm{L}} B_{\mathrm{T}} (E^*_i, \mathbf{p}^*_i), \tag{49}$$

where B_{L} and B_{T} are the boosts defined in Eq. (17). The effect of these boosts on the momenta of the decay pions from a ρ is illustrated in Fig. 6.

D. Spin density matrix of q'

When a VM has been generated by the splitting $q \to \mathrm{VM} + q'$, the information about the spin state of q', encoded in its density matrix $\hat{\rho}(q') = (\mathbf{1} + \boldsymbol{\sigma}\cdot\mathbf{S}_{q'})/2$, depends on the information about the decay products of the VM.

1. Case without information about the decay products

Suppose that the VM is not analyzed (only p is recorded, not the momenta of the decay products). Then

$$\hat{\rho}(q') = \left[\sum_{\mathbf{V}=\mathbf{l},\mathbf{m},\mathbf{n}} T(\mathfrak{q}', \mathfrak{h}, \mathfrak{q}) \hat{\rho}(q) T^\dagger(\mathfrak{q}', \mathfrak{h}, \mathfrak{q})\right] / \mathrm{Tr}[\cdots],$$
$$= \frac{(\mu + \sigma_z \boldsymbol{\sigma}\cdot\mathbf{k}'_{\mathrm{T}}) \Gamma_{h,\alpha} \hat{\rho}(q) \Gamma^\dagger_{h,\alpha} (\mu^* + \boldsymbol{\sigma}\cdot\mathbf{k}'_{\mathrm{T}}\sigma_z)}{(|\mu|^2 + \mathbf{k}'^2_{\mathrm{T}}) N(\mathbf{S}_q)}, \tag{50}$$

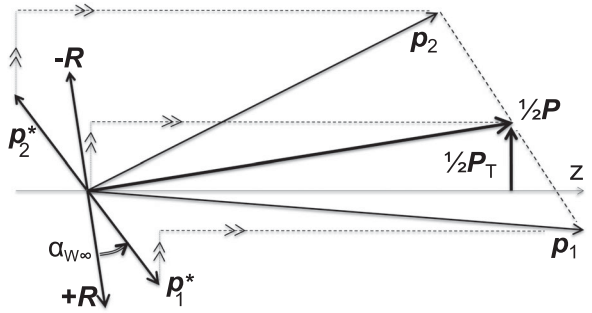

FIG. 6. Boosts transforming the pion momenta of ρ decay, from the LR symmetric frame ($\mathbf{p}_1^* = \mathbf{r}$ and $\mathbf{p}_2^* = -\mathbf{r}$) to the string frame ($\mathbf{p}_1$ and $\mathbf{p}_2$). Also shown is the relative momentum $\mathbf{R}$ in the null-plane frame, related to $\mathbf{r}$ by a Wigner rotation of angle $\alpha_{W\infty}$. The line "….≫…." represents the move of the extremity of a vector $\mathbf{p}$ during the boosts B_T and B_L. The figure is calculated for $|\mathbf{p}_T|/M_\rho = 8/15$, $P_L/\epsilon(\rho) = 35/12$, and $\mathbf{p}_1$ and $\mathbf{p}_2$ in the $(\hat{\mathbf{z}}, \mathbf{p}_T)$ plane.

where $[\cdots]$ repeats the numerator. The second expression looks like in Eq. (31), but summing over $\alpha = \alpha'$ and removing the symbol Tr in the numerator.

For the emission of a pseudoscalar meson, the spin density matrix of q' can be calculated using Eq. (50) with $\Gamma_h = \sigma_z$ as in M19 [22].

Depolarization of the recurring quark.—As in the model with only pseudoscalar mesons [cf. Eqs. (31)–(32) of [22]], the recurring quark becomes less and less polarized as its rank increases, if the transverse momenta of the emitted hadrons are integrated over. The depolarization coefficients $D_{TT}^{VM} \equiv \mathbf{S}_{q'T}/\mathbf{S}_{qT}$ and $D_{LL}^{VM} \equiv S_{q'L}/S_{qL}$ following the emission of a VM are obtained by replacing the numerator and the denominator of Eq. (50) by their averages on $\mathbf{k}'_T$ weighted by $f_T^2(\mathbf{k}'_T)$:

$$D_{TT}^{VM} = f_L(1 + \langle \mathbf{k}_T^2 \rangle_{f_T}/|\mu|^2)^{-1} = -f_L D_{TT}^{PS},$$
$$D_{LL}^{VM} = (2f_L - 1)\frac{|\mu|^2 - \langle \mathbf{k}_T^2 \rangle_{f_T}}{|\mu|^2 + \langle \mathbf{k}_T^2 \rangle_{f_T}} = (2f_L - 1)D_{LL}^{PS}, \quad (51)$$

where D_{TT}^{PS} and D_{LL}^{PS} are given in Eqs. (31)–(32) of [22]. Note that these coefficients are smaller for VM than for PS. This is due to the loss of information when the momenta of the decay products are not measured. Note also the opposite signs of D_{TT}^{VM} and D_{TT}^{PS}.

2. Case where the momenta of decay products are known

The VM decay matrix.—As already said, $\hat{\rho}(q')$ depends on the information about the decay products of the VM. This information is encoded in a matrix $\check{\rho}(h)$ called the *decay matrix* (also indicated with D in literature) [29,30] or *acceptance (density) matrix* [35]. $\check{\rho}(h)$ can be seen as the density matrix of the VM running backward in time, contrary to the *emittance* density matrix $\hat{\rho}(h)$ studied in Sec. II B. For a definite state $|\mathbf{p}_1^*, \mathbf{p}_2^* \cdots\rangle$ of the decay products,

$$\check{\rho}_{\alpha'\alpha}(h) = \mathcal{M}_{\alpha'}^\dagger(p_1, p_2 \cdots)\mathcal{M}_\alpha(p_1, p_2 \cdots), \quad (52)$$

writing the decay amplitude as $\mathcal{M}_\alpha(p_1, p_2 \cdots)V_\alpha$. For the decays that we consider,

$$\check{\rho}_{\alpha'\alpha}(h) \propto \begin{cases} \hat{\mathbf{r}}_{\alpha'}\hat{\mathbf{r}}_\alpha & (\mathrm{VM} \to 2\mathrm{PS}) \\ \hat{\boldsymbol{\tau}}_{\alpha'}\hat{\boldsymbol{\tau}}_\alpha & (\mathrm{VM} \to 3\mathrm{PS}) \\ \delta_{\alpha\alpha'} - \hat{\mathbf{r}}_\alpha\hat{\mathbf{r}}_{\alpha'} & (\omega \to \pi^0\gamma) \\ \delta_{\alpha\alpha'} & (\mathrm{VM\ not\ analyzed}) \end{cases}. \quad (53)$$

We write "$\propto$" instead of "=" because we do not fix the trace of $\check{\rho}(h)$. The angular distribution in Eq. (39) or in Eq. (43) is proportional to $\mathrm{Tr}\{\hat{\rho}(h)\check{\rho}(h)\}$. In the third line of Eq. (53), the decay state is an incoherent superposition of the states with photon helicities ± 1. The last line is for the case where $\hat{\mathbf{r}}$ or $\hat{\mathbf{n}}$ is not recorded. In lines 1 and 2, $\check{\rho}(h)$ is the density matrix of a pure state, instead in lines 3 and 4 it is that of a statistical mixture.

Combining $\check{\rho}(h)$ and $\hat{\rho}(q)$.—Taking into account the information encoded in $\check{\rho}(h)$, we replace Eq. (50) by

$$\begin{aligned}\hat{\rho}(q') &\propto T_\alpha \rho(q) T_{\alpha'}^\dagger \check{\rho}_{\alpha'\alpha}(h) \\ &\propto (\mu + \sigma_z \boldsymbol{\sigma}\cdot\mathbf{k}'_T)\Gamma_{h,\alpha}\hat{\rho}(q) \\ &\quad \times \Gamma_{h,\alpha'}^\dagger \check{\rho}_{\alpha'\alpha}(h)(\mu^* + \boldsymbol{\sigma}\cdot\mathbf{k}'_T\sigma_z). \end{aligned} \quad (54)$$

Compared to Eq. (50), there are two indices α and α', which we contract with those of $\check{\rho}_{\alpha'\alpha}(h)$. Again the use of "$\propto$" instead of "=" means that we have not yet fixed the trace of $\hat{\rho}(q')$.

Note.—Carrying information "backward in time" with $\check{\rho}(h)$ is necessary to generate the correct correlations between the spin of q' and the momenta of the decay products when the joint density matrix

$$\langle\alpha| \otimes \langle s_{q'}|\hat{\rho}(h, q')|s'_{q'}\rangle \otimes |\alpha'\rangle = \langle s_{q'}|T_\alpha \hat{\rho}(q) T_{\alpha'}^\dagger|s'_{q'}\rangle \quad (55)$$

is entangled. This is the general case: for instance, if q is in the pure spin state $|\mathbf{S}_q = +\hat{\mathbf{y}}\rangle$, the VM + q' system is in the entangled (nonseparable) state

$$\begin{aligned}\sum_\alpha |\alpha\rangle \otimes T_\alpha|\mathbf{S}_q\rangle &\propto G_T[|\mathbf{x}\rangle \otimes \sigma_x|\hat{\mathbf{y}}\rangle + |\mathbf{y}\rangle \otimes \sigma_y|\hat{\mathbf{y}}\rangle] \\ &+ G_L|\mathbf{z}\rangle \otimes |\hat{\mathbf{y}}\rangle = G_T|\mathbf{x}\rangle \otimes |-\hat{\mathbf{y}}\rangle + [G_T|\mathbf{y}\rangle + G_L|\mathbf{z}\rangle] \otimes |\hat{\mathbf{y}}\rangle. \end{aligned} \quad (56)$$

III. MONTE CARLO IMPLEMENTATION

The structure of the stand alone MC implementation of M20 is the same as that of M19 [22]. First the flavor u, d,

or s, the four-momentum and the spin density matrix of the fragmenting quark q_A are defined. In the simulations of the fragmentation process in a SIDIS event the initial quark energy has been taken from a sample of SIDIS events collected by the COMPASS experiment with a 160 GeV/c muon beam, and having $Q^2 > 1$ (GeV/c)^2 and the invariant mass of the final hadronic system larger than 5 GeV/c^2, as in Ref. [22]. For the comparison with e^+e^- data a fixed center of mass energy $\sqrt{s} = 10$ GeV has been used to compare with the BELLE experiment. Once the initial quark state has been set up, the fragmentation chain is simulated by repeating recursively the elementary splitting $q \to h + q'$ until the condition for the termination of the fragmentation chain is reached. The hadron h is assigned to the vector or pseudoscalar multiplet according to the relative probability $f_{\mathrm{VM/PS}}$. This parameter is fixed and taken as in PYTHIA8, namely for light mesons containing only u and d quarks it is $f_{\mathrm{VM/PS}} = 0.62$ whereas for mesons containing at least one strange quark it is $f_{\mathrm{VM/PS}} = 0.725$.

The simulation of the elementary splittings in M20 proceeds in the following steps:

(1) Generate a new $q'\bar{q}'$ pair with $q' = u, d, s$ taking into account the suppression of s quarks according to the relative probabilities $P(u\bar{u}):P(d\bar{d}):P(s\bar{s}) = 3/7:3/7:1/7$ as in [22] with M19.

(2) Form $h = q\bar{q}'$ and choose the VM multiplet with probability $f_{\mathrm{VM/PS}}/(1 + f_{\mathrm{VM/PS}})$. If $(q\bar{q}')$ is flavor neutral, then choose the meson species h with probability proportional to $|C_{q',h,q}|^2$, according to Eqs. (13) and (16). If h is PS, then assign the corresponding mass. If h is a VM, then generate its mass M with the $|D_h(M)|^2$ distribution, according to Eq. (29) summed over $\mathbf{V}$ and integrated over Z and $\mathbf{k}'_{\mathrm{T}}$.

(3) According to Eqs. (27) and (29) generate $\mathbf{k}'^2_{\mathrm{T}}$ with the distribution $f_{\mathrm{T}}^2(\mathbf{k}'^2_{\mathrm{T}})(|\mu|^2 + \mathbf{k}'^2_{\mathrm{T}})/\langle|\mu|^2 + \mathbf{k}'^2_{\mathrm{T}}\rangle_{f_{\mathrm{T}}}$, and the azimuthal angle $\phi(\mathbf{k}'_{\mathrm{T}})$ following the factor $(1 + \hat{a}S_n)$ for a PS, $(1 - f_{\mathrm{L}}\hat{a}S_n)$ for a VM. Construct $\mathbf{p}_{\mathrm{T}} = \mathbf{k}_{\mathrm{T}} - \mathbf{k}'_{\mathrm{T}}$ (with $\mathbf{k}_{\mathrm{T}} = 0$ for $q = q_A$).

(4) Generate Z with the distribution given in the second line of Eq. (27) or third line of Eq. (29).

(5) Calculate $p^+ = Zk^+$, p^- imposing the mass shell condition $p^+p^- = \epsilon^2$ and $k'^{\pm} = k^{\pm} - p^{\pm}$.

(6) Test the exit condition (see below) on the remaining mass squared $M_{\mathrm{X}}^2 = (k' + k_B)^2$. If it is not satisfied, then continue with the next step, otherwise the current hadron is removed and the fragmentation chain ends. We do not treat the decay of the remaining string piece.

(7) Construct the hadron four-momentum $p = (E, \mathbf{p}_{\mathrm{T}}, p_z)$ by calculating $E = (p^+ + p^-)/2$ and $p_z = (p^+ - p^-)/2$. Store the hadron in the event record.

(8) If h is a PS calculate the spin density matrix of q' using Eq. (50) with $\Gamma_h = \sigma_z$ and return to step (1). If h is a VM, then do the following:
   (i) Calculate the spin density matrix $\hat{\rho}(h)$ of h using Eq. (31).
   (ii) Chose the decay channel (if more than one) as specified below. Construct the momenta of the decay hadrons using $\hat{\rho}(h)$ to generate the angles as explained in Sec. II C.
   (iii) Boost the decay products according to Eq. (49). Store the decay hadrons in the event record.
   (iv) Build the acceptance matrix $\check{\rho}(h)$ of Eq. (53).
   (v) Calculate the spin density matrix of q' using Eq. (54). Go to step 1.

The probabilities used to determine the PS meson species at step (2) are the same as in M19. The probabilities of the VM species are obtained from the corresponding wave functions in flavor space. Unlike the PS case, for VM production there is no suppression factor among flavor neutral states, e.g., a spin-1 $u\bar{u}$ or $d\bar{d}$ pair is assigned to a ρ^0 or to an ω with the same probability (see also Ref. [28]).

The exit condition in step 6 is satisfied when not enough remaining mass squared is left in the string to produce at least one resonance (baryonic in SIDIS, mesonic in e^+e^-) as in M19.

The decay channels considered in (8.2) are $\rho \to \pi\pi$, $K^* \to K\pi$, $\omega \to \pi^+\pi^-\pi^0$, $\omega \to \pi^0\gamma$, $\omega \to \pi^+\pi^-$, $\phi \to K^+K^-$, $\phi \to K^0_S K^0_L$, $\phi \to \pi^+\pi^-\pi^0$, $\phi \to \eta\gamma$, and $\phi \to \pi^0\gamma$. The corresponding branching ratios are taken from the PDG [32]. In the case of the $K^* \to K\pi$ decay, we take the branching ratios given by isospin symmetry, e.g., $K^{*0} \to K^+\pi^-$ with branching ratio 2/3 and $K^{*0} \to K^0\pi^0$ with branching ratio 1/3. Concerning K^0 and $\bar{K}^0$ we keep the quantum state as it is immediately after emission without evolving with mixing and oscillations.

IV. RESULTS OF SIDIS SIMULATIONS

This section is dedicated to the results obtained from the Monte Carlo simulations of the fragmentation of u quarks with full transverse polarization along the $\mathbf{Y}$ axis (hence $|\mathbf{S}_{q_A\mathrm{T}}| = 1$). Results for d quarks can be deduced from isospin and charge conjugation arguments. The primordial transverse momentum of the fragmenting quark has been switched off. Its effect on transverse spin asymmetries was studied for M18 in Ref. [21].

Concerning the free parameters of the model a, b_{L}, b_{T}, and μ, the same values as in M19 are used, namely $a = 0.9$, $b_{\mathrm{L}} = 0.5(\mathrm{GeV}/c^2)^{-2})$, $b_{\mathrm{T}} = 5.17(\mathrm{GeV}/c)^{-2}$, and $\mu = (0.42 + i0.76)$ GeV/c^2. For the two new free parameters, we take first $|G_{\mathrm{L}}/G_{\mathrm{T}}| = 1$ (i.e., $f_{\mathrm{L}} = 1/3$) and $\theta_{\mathrm{LT}} = 0$, in agreement with Ref. [27] (see the text concerning Fig. 10). The sensitivity of the observables on the values of the new parameters is then discussed in Sec. IV C.

A. Kinematic distributions

In the study of the distributions of the hadrons fractional energy z and transverse momentum p_T we apply the cuts $p_T > 0.1$ GeV/c when looking at the z distribution, and $z > 0.2$ when looking at the p_T distribution, in analogy with real data analyses.

In the top row of Fig. 7 we compare the z (left plots) and p_T (right plots) distributions for the primary π^+, the ρ^+ and the π^+ produced in ρ^+ decays. The analog distributions for π^- and ρ^- are given in the bottom row.

As can be seen, vector mesons carry typically larger fractions of the initial quark energy than primary pseudoscalar mesons. It is due to the exponential factor in Eq. (27) which favors large Z for large M.

Concerning the p_T distributions, VMs have typically smaller transverse momenta than primary PS mesons. This is due to the hidden spin effect described in Fig. 3: for rank $r \geq 2$ in the string $+ {}^3P_0$ model the transverse momenta of the quarks that constitute the vector meson have on the average opposite directions while in the pseudoscalar case where they lay along the same direction. We have then $\langle \mathbf{p}_T^2 \rangle_{VM} < 2\langle \mathbf{k}_T^2 \rangle < \langle \mathbf{p}_T^2 \rangle_{PS}$. This is at variance with PYTHIA, where the Z-integrated splitting function is the same for vector mesons and for primary pseudoscalar mesons.

Coming to PS mesons from a VM decay, they carry smaller fractional energies and comparable transverse momenta with respect to their parent. They inherit only part of the parent transverse momentum, but to this is added a contribution from the PS momentum $\mathbf{p}_{iT}^*$ in the VM rest frame, following Eq. (34).

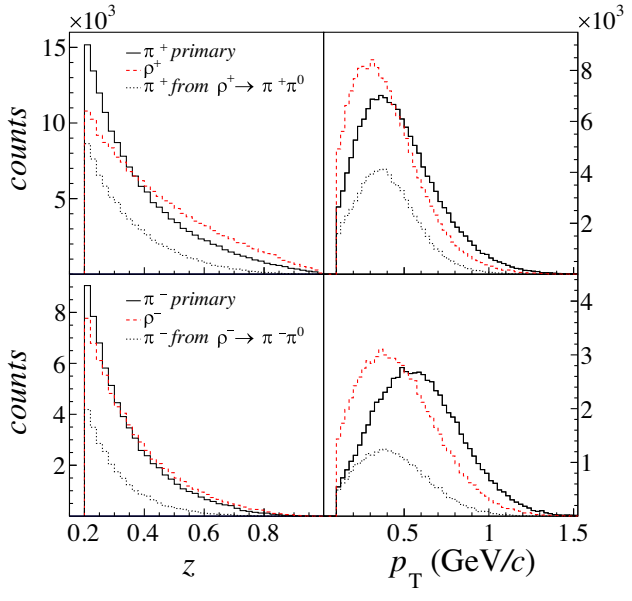

FIG. 7. Upper row: comparison between the z (left) and p_T (right) distributions for primary π^+ (continuous histogram), ρ^+ (dashed histogram) and π^+ from the ρ^+ decay (dotted histogram). Lower row: same distributions for π^- and ρ^-. $G_L \equiv G_T$ case.

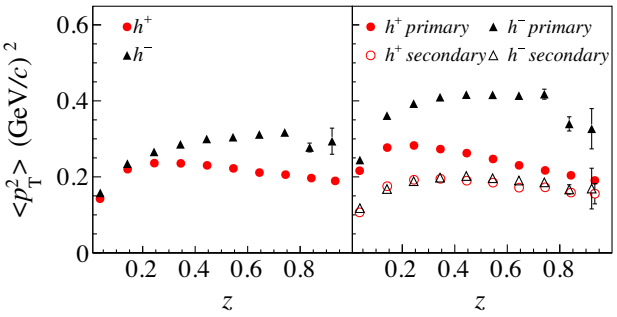

FIG. 8. Left panel: $\langle \mathbf{p}_T^2 \rangle$ as function of z for positive (circles) and negative (triangles) hadrons. Right panel: same for primary (closed markers) and secondary (open markers) positive (circles) and negative (triangles) hadrons. $G_L \equiv G_T$ case.

The hierarchy among the transverse momenta of the different final hadrons is more clearly seen in Fig. 8. The left panel shows $\langle \mathbf{p}_T^2 \rangle$, namely the mean of the $\mathbf{p}_T^2$ distribution, as function of z for positive and negative hadrons. The same quantity for primary and secondary (from VM decay) mesons is shown in the right panel. Among the primary mesons, the negative ones have larger transverse momenta than the positive ones, as expected from recursive fragmentation models and discussed in Ref. [22]. Positive and negative secondary mesons, instead, have nearly the same $\langle \mathbf{p}_T^2 \rangle$, thus the large difference between the positive and negative hadrons at large z is reduced when looking at all hadrons but it is still there, at variance with the experimental data [37].

Figure 9 shows the fraction of secondary charged hadrons as function of z and of p_T in the final sample. Again, the contribution of VM decay decreases with z. Also, the fraction of the secondary mesons is large at $p_T < 0.5$ (GeV/c), rising up to 0.8 for negative hadrons at small transverse momenta.

B. Transverse spin asymmetries

1. Collins asymmetry

In the fragmentation process of transversely polarized quarks, the final state hadrons are produced with an

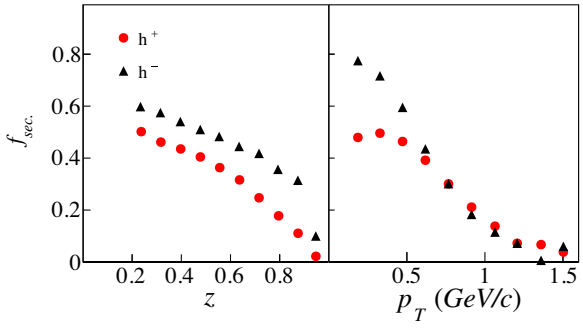

FIG. 9. Fraction of secondary positive (circles) and negative (triangles) hadrons produced in decays of vector mesons as function of z (left panel) and p_T (right panel). $G_L \equiv G_T$ case.

azimuthal distribution given in Eq. (1). When looking at the simulated events, the Collins analyzing power $a^{q\uparrow\to h+X}$ is extracted as

$$a^{q_A\uparrow\to h+X}(z,p_T)=2\frac{\langle\sin(\phi_h-\phi_{S_{q_A}})\rangle}{|\mathbf{S}_{q_AT}|}. \quad (57)$$

It has been studied as function of the hadron rank r, of the fractional energy z and of the transverse momentum p_T for primary and secondary PS and for VM. Also, we apply the kinematic cuts $z>0.2$ (when looking at p_T) and $p_T>0.1$ GeV/c. We remind that for these simulations the values $|G_L/G_T|=1$ and $\theta_{LT}=0$ have been used and that other choices give different Collins analyzing powers, as will be shown in Sec. IV C.

Figure 10 shows the rank dependence of the Collins analyzing power for primary π^+ and for ρ^+. It is compared with the analyzing power for π^+ from M19. Rank one ρ^+ have a Collins analyzing power of opposite sign with respect to rank one π^+ and a factor of 3 smaller. This is expected when combining Eq. (27) with (29), which gives for the rank 1 the relation $a^{u\uparrow\to VM+X}/a^{u\uparrow\to PS+X}=-f_L$. For $|G_L/G_T|=1$ this ratio is $-1/3$ [27]. For $r\geq 2$ the ρ^+ analyzing power has the same sign as the π^+ analyzing power but is smaller. Indeed, both for VM and PS with $r\geq 2$, $\mathbf{p}_T$ is more likely on the same side as $\mathbf{k}_T$, but it is reduced by $\mathbf{k}'_T$ for a VM polarized in the $(\hat{\mathbf{z}},\mathbf{p}_T)$ plane. Also, the analyzing power of π^+ mesons decays faster with the rank as compared to M19. This is expected from the opposite signs of the D_{TT} depolarization factors and from the fact that, for a given rank, the number of antecedent PS mesons is not fixed.

Coming back to the observable quantities, Fig. 11 shows the rank-averaged Collins analyzing power as function of z (left panel) and as a function of p_T (right panel) for ρ^+ and π^+ produced in the ρ^+ decay. The ρ^+ analyzing power is positive as expected from Fig. 10. The analyzing power of the decay π^+, inherited from the ρ^+, exceeds the ρ^+ one at large z. This is due to the fact that large z decay pions come

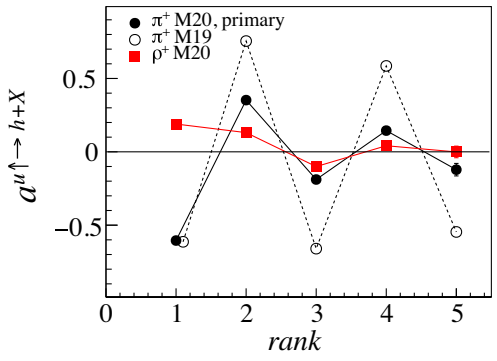

FIG. 10. Comparison between the Collins analyzing power as function of rank for π^+ from M19 (open circles), primary π^+ from M20 (closed circles) and ρ^+ (squares). $G_L\equiv G_T$ case.

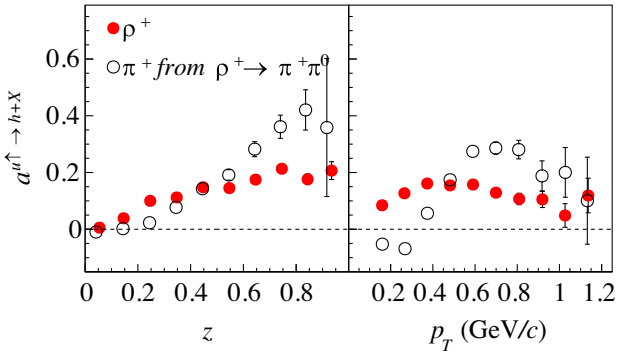

FIG. 11. Comparison between the Collins analyzing power as function of z (left panel) and as function of p_T (right panel) for ρ^+ (closed points) and the analyzing power of π^+ produced in the decay $\rho^+\to\pi^+\pi^0$ (open points). $G_L\equiv G_T$ case.

mostly from longitudinally polarized vector mesons, which have an analyzing power three times larger than the not analyzed ones, according to Eq. (29) with $f_L=1/3$. Looking at the p_T dependence, decay π^+ have negative analyzing power at low p_T that becomes positive at large p_T. This is due to the fact that decay π^+ with large p_T can be produced from a rank one ρ^+ polarized along $\mathbf{M}$ or from rank ≥ 2 ρ^+ polarized along $\mathbf{N}$. In the former case, the transverse momentum that the pion acquires in the decay adds constructively [see Eq. (34)] to the transverse momentum inherited from the ρ^+, which has positive analyzing power. In the latter case, the ρ^+ has a large transverse momentum and the same Collins analyzing power as a PS meson [see Eq. (29)]. The negative analyzing power of the decay π^+ at low p_T is interesting. It is probably due to pions which have a transverse velocity in the ρ^+ rest frame larger than, but opposite to, the transverse velocity of the ρ^+ in the string rest frame.

The π^0 produced in the same decay has the same analyzing power as the positive pion because of parity invariance. With the present choice of parameters, the ρ^0 and ρ^- mesons have a similar analyzing power as ρ^+ and the same features are seen also in the decay of ρ^- and ρ^0 mesons.

The effects of the decays of different VMs have been investigated separately. The results are summarized in Table I where the integrated analyzing power for positive and negative pions is given for all decays switched off, after switching on the ρ meson decays separately or at the same time, and after switching on VM decays. The corresponding values of the analyzing power as obtained with the model M19 are also given. From Table I one can see that primary π^+ in M20 have larger analyzing power than π^+ in M19 while the reverse is true for π^-. This is due to the fact that rank two primary pions in M20 have smaller analyzing power than in M19, as shown in Fig. 10. The largest reduction of the analyzing power comes from decays of ρ mesons while switching on ω, K^*, and ϕ decays does not have a large impact. All things considered, after switching

TABLE I. Average values of Collins analyzing power for charged pions obtained with M20 and M19. For each hadron the cuts $z > 0.2$ and $p_T > 0.1$ GeV/c have been applied. $G_L \equiv G_T$ case.

M20	$\langle a^{u\uparrow\to\pi^+ +X}\rangle$	$\langle a^{u\uparrow\to\pi^- +X}\rangle$
No VM decay	-0.308 ± 0.003	0.218 ± 0.005
With ρ^+ decays	-0.178 ± 0.003	0.216 ± 0.005
With ρ^- decays	-0.307 ± 0.003	0.172 ± 0.004
With ρ^0 decays	-0.210 ± 0.003	0.151 ± 0.004
With $\rho^{\pm,0}$ decays	-0.136 ± 0.003	0.140 ± 0.004
With all VM decays	-0.124 ± 0.003	0.124 ± 0.003
M19	-0.251 ± 0.004	0.257 ± 0.006

on decays of all VMs the analyzing power of charged pions is reduced by a factor of two compared to M19. It is also important to note that in this model the absolute values of the analyzing power of π^+ and π^- are different if restricted to primary mesons, but after switching on vector meson decays they become the same, as it is the case also in M19 and as seen in the experimental data [38].

The effect of vector mesons on the π^+ and π^- Collins analyzing power is shown in Fig. 12 where the analyzing powers for charged pions obtained with M20, when the decays of all VMs are simulated, and with M19 are compared. The effect is large for both charges and as function of z and of p_T. The z dependence of the π^+ analyzing power is not linear any longer, at variance with M19.

The same considerations hold for the analyzing power of charged kaons. In this case, the effect of vector mesons is smaller than for pions.

2. Dihadron asymmetry

Dihadron transverse spin asymmetries are studied looking at hadron pairs h_1h_2, where 1 (2) refer to the positive (negative) charged hadron. The azimuthal angle ϕ_R of $\mathbf{R}_T$ is distributed according to

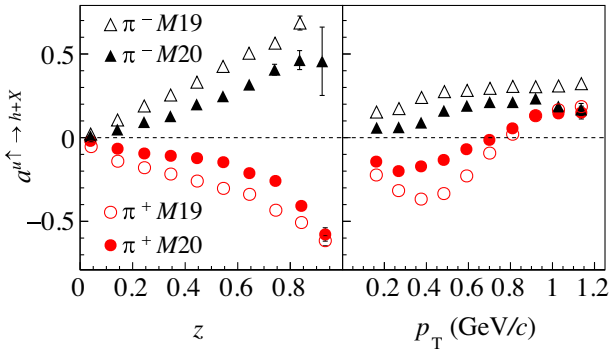

FIG. 12. The Collins analyzing power of positive (circles) and negative (triangle) pions as function of z (left panel) and of p_T (right panel). The closed (open) markers are obtained with M20 (M19). $G_L \equiv G_T$ case.

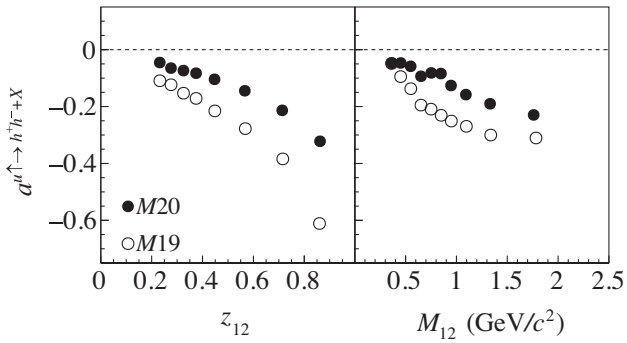

FIG. 13. Dihadron analyzing power for charged pions as function of z_{12} (left panel) and M_{12} (right panel), as obtained with M19 (open markers) and with M20 (closed markers). $G_L \equiv G_T$ case.

$$\frac{d^3N_{hh}}{dz_{12}dM_{12}d\phi_R} \propto 1 + a^{q\uparrow\to h_1h_2+X}|\mathbf{S}_{q_A T}|\sin(\phi_R - \phi_{S_{q_A}}). \tag{58}$$

The dihadron analyzing power $a^{q\uparrow\to h_1h_2+X}$ is calculated as $2\langle\sin(\phi_R - \phi_{S_{q_A}})\rangle/|\mathbf{S}_{q_A T}|$ averaged on $|\mathbf{R}_T|$. It has been evaluated as functions of the fractional energy $z_{12} = z_1 + z_2$ and the invariant mass M_{12} of the pair. In addition for each hadron of the pair we apply the kinematic cuts $z > 0.1$, $x_F > 0.1$ and we ask for $R_T > 0.07$ GeV/c, in analogy with the COMPASS analysis [39]. The Feynman x_F variable is defined as $x_F = 2p^z_{cm}/\sqrt{s}$, with p^z_{cm} being the hadron longitudinal momentum in the string rest frame.

The result for is shown in Fig. 13 as function of z_{12} and M_{12} when switching on the decays of all vector mesons. The comparison with the dihadron analyzing power obtained by M19 is shown there and summarized in Table II. We see that the introduction of VMs reduces the analyzing power obtained with only PS mesons in M19 by more than a factor of two. One reason is that the dihadron asymmetry is strongly linked to the Collins effect [38] and the latter is smaller for M20 than for M19 (see Fig. 12). The other reason is that the VM decay process is invariant by $\mathbf{R} \to -\mathbf{R}$, thus secondary mesons do not contribute to this dihadron analyzing power. Instead, they dilute it. We note also that both in M19 and in M20 the average values of the dihadron and the Collins analyzing powers are comparable, like in the experimental result [38]. Still it must be reminded that these results are obtained without primordial transverse momentum, which reduces

TABLE II. Average values of dihadron analyzing power for charged pions obtained with M19 and with M20. $G_L \equiv G_T$ case.

Model	$\langle a^{q\uparrow\to\pi^+\pi^- +X}\rangle$
M19	-0.246 ± 0.005
M20	-0.111 ± 0.005

the Collins analyzing power but does not affect the dihadron analyzing power [21].

C. Case of $|G_L| \neq |G_T|$ and $\theta_{LT} \neq 0$

In this subsection and in Sec. V we show the effect of changing the values of the parameters $|G_L/G_T|$ and θ_{LT} on the relevant observables, namely kinematic distributions and spin asymmetries. We have selected three values for $|G_L/G_T|$: 5, 1, and 1/5, corresponding to $f_L = 0.93$, $f_L = 1/3$, and $f_L = 0.02$. For each value of $|G_L/G_T|$ we set $\theta_{LT} = -\pi/2$, $\theta_{LT} = 0$, and $\theta_{LT} = +\pi/2$. The values $\theta_{LT} = \pm\pi/2$ maximize the oblique polarization, whereas $\theta_{LT} = 0$ gives no oblique polarization (in the LR symmetric frame) as can be seen from Eq. (33). The values of the other parameters are the same as given in the previous section.

1. Effect on the kinematic distributions

The effect of changing the values of $|G_L/G_T|$ and θ_{LT} on the z and p_T distributions of the produced hadrons is small and is not shown here. More sizeable effects can be seen in the kinematic distributions of hadron pairs.

Figure 14 shows the M_{12} distribution for hadrons coming from decays of vector mesons (left panel) and for all hadrons (right panel), for the parameter values $|G_L/G_T| = 5, 1, 1/5$. The parameter θ_{LT} has a weaker influence and it is set to zero. The peaks corresponding to the decays $\rho^0 \to \pi\pi$, $\phi \to KK$, and $K^* \to K\pi$ can be seen. The shoulder visible on the left of the ρ^0 peak is due to the decay $\omega \to \pi\pi\pi$. In the left panel, it is clearly seen that the peaks corresponding to ρ^0, K^*, and ϕ decrease by increasing $|G_L/G_T|$. This is due to the p_T and z cuts applied to the decay products which make the "acceptance" for VMs depend on its polarization, therefore on these parameters. In fact, in the 2-body decay of a longitudinally polarized vector meson one of the decay products has a low z and can easily be rejected when applying the cut $z > 0.1$. One the contrary, the ω shoulder increases with $|G_L/G_T|$, due to the fact that the decay pions of a ω are emitted preferentially perpendicular, instead of parallel, to the linear polarization of the ω [see Eq. (41)].

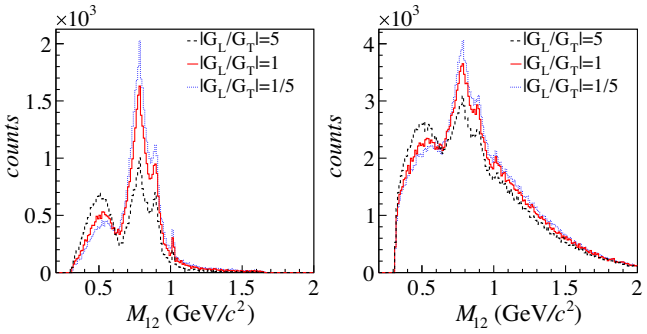

FIG. 14. Distributions of M_{12} for h^+h^- produced in VM decays (left panel) and for all pairs (right panel), for $|G_L/G_T| = 5$ (dashed line), $|G_L/G_T| = 1$ (continuous line) and $|G_L/G_T| = 1/5$ (dotted line), and $\theta_{LT} = 0$.

These effects can be seen also in the invariant mass distribution of all hadron pairs, shown in the right panel of Fig. 14. In this case, another contribution to the increase of the shoulder on the left of the ρ^0 region for $|G_L/G_T| = 5$ is given by pairs of hadrons from the combinatorial background. Indeed, the decay pions of a longitudinal ρ are separated in rapidity from their parent by typically more than one unit and can be easily associated with other pions to form low mass pairs. For $|G_L/G_T| = 1$ the invariant mass distribution is similar to that obtained with PYTHIA. Instead, comparing with the distribution measured in SIDIS (see, e.g., Ref. [39]), the combinatorial background is lower than in the data.

From these examples it is clear that the VM polarization has a non negligible role in the "spin-independent" kinematic distributions of the observed hadron pairs, when the experimental cuts are applied, and should be taken into account in the description of all fragmentation processes, the quark being polarized or not.

2. Effect on the transverse spin asymmetries

In this paragraph we consider the Collins effects for the VMs ("global Collins effect") and for their decay products. The effects on the dihadron asymmetries are illustrated in Sec. V.

The effect of varying the value of $|G_L/G_T|$ on the Collins analyzing power of ρ^+, ρ^0, and ρ^- mesons is shown in Fig. 15. The parameter θ_{LT} does not affect the global Collins analyzing power of vector mesons and is set to zero. In each row the analyzing power is given as function of z (left plot) and of p_T (right plot). To interpret these results it is useful to look at the production of rank 1 and 2 VMs in the classical string + $^3P_0$ model illustrated in Fig. 16 for $|G_L/G_T| \gg 1$ (upper part) and $|G_L/G_T| \ll 1$ (lower part). Each diagram shows the application of the $^3P_0$ mechanism to the production of VMs polarized along **Z** (upper part), and **X** or **Y** (lower part) for an initial quark polarized along **Y**.

As it can be seen in Fig. 15, varying $|G_L/G_T|$ produces large effects for all ρ mesons. In particular for $|G_L/G_T| = 5$ the Collins analyzing power of ρ^+ mesons as function of z is large rising up to 0.5. It is then dominated by the rank one diagram (1) in Fig. 16. Rank one longitudinally polarized ρ^+ have opposite but equal in magnitude analyzing power compared to rank 1 PS meson [compare Eqs. (27) and (29)]. For low values of $|G_L/G_T|$ the analyzing power of ρ^+ mesons is reduced due to the presence of two transverse polarization states with opposite analyzing powers [diagrams (2) and (3) in Fig. 16].

Concerning ρ^-, its analyzing power is small at large $|G_L/G_T|$ and it increases at small $|G_L/G_T|$, becoming larger than ρ^+ and ρ^0 for $|G_L/G_T| = 1/5$. For $|G_L/G_T| = 5$ the analyzing power is in fact dominated by diagrams (4)

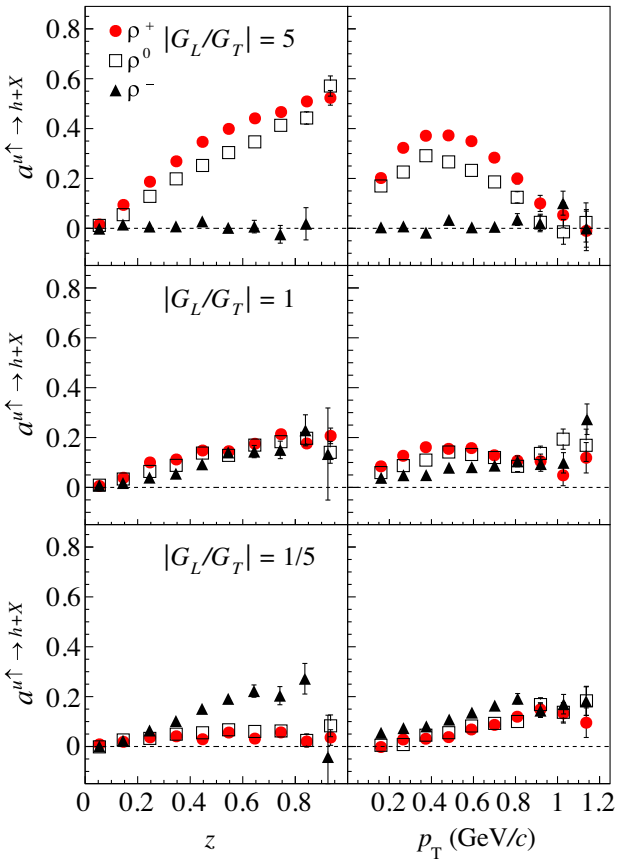

FIG. 15. Collins analyzing power for ρ^+ (circles), ρ^0 (squares), and ρ^- (triangles) as function of z (left plots) and of p_{T} (right plot). The upper row is obtained with $|G_{\mathrm{L}}/G_{\mathrm{T}}| = 5$, the middle row with $|G_{\mathrm{L}}/G_{\mathrm{T}}| = 1$ and the lower row with $|G_{\mathrm{L}}/G_{\mathrm{T}}| = 1/5$. The parameter θ_{LT} is taken zero.

and (5) in Fig. 16, which have opposite signs. For $|G_{\mathrm{L}}/G_{\mathrm{T}}| = 1/5$ the asymmetry is essentially given by diagrams (7) and (6) associated to rank one PS. When associated to rank one VM, (6) and (7) are canceled by (8) and (9). For $|G_{\mathrm{L}}/G_{\mathrm{T}}| = 1$ the analyzing power of all ρ mesons are very similar, as already mentioned. Also the analyzing power for ρ^0 mesons is the weighted average of the analyzing powers for ρ^+ and ρ^- due to isospin invariance of the production amplitude.

The effect as function of p_{T} is also strong for ρ^+ and ρ^0, which for $|G_{\mathrm{L}}/G_{\mathrm{T}}| = 5$ behave similarly to PS mesons but with opposite analyzing power. Decreasing $|G_{\mathrm{L}}/G_{\mathrm{T}}|$, transverse polarization states become dominant and the shape of the analyzing power is changed. At large p_{T} ρ mesons are mostly rank 2 polarized along **N** and the analyzing power is essentially given, in Fig. 16, by the diagram (7) associated to a rank one PS. When associated to a rank one VM, diagrams (7) and (9) cancel each other, only contributing to dilute the effect.

The parameter θ_{LT} has little influence on the global Collins effect of the resonance, as said before, but a strong influence on the Collins effects of the decay products.

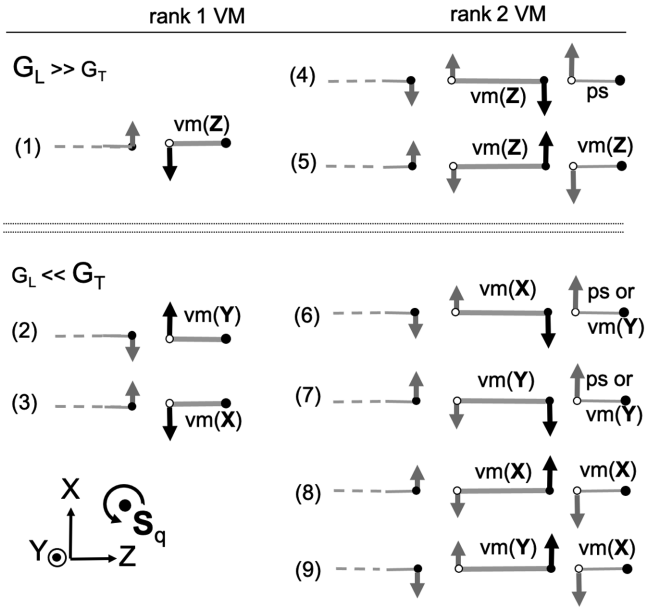

FIG. 16. Classical string + $^3P_0$ picture applied to the production of rank 1 (left diagrams) and 2 (right diagrams) vector mesons for $|G_{\mathrm{L}}/G_{\mathrm{T}}| \gg 1$ (upper part) and $|G_{\mathrm{L}}/G_{\mathrm{T}}| \ll 1$ (lower part). The quark q_A is polarized along **Y**; vm(**X**), for instance, indicates a VM polarized along **X**.

This is seen in Fig. 17, which shows the analyzing power of π^+ produced in $\rho^+ \to \pi^0\pi^+$ decays, for $\theta_{\mathrm{LT}} = -\pi/2, 0, +\pi/2$ and $|G_{\mathrm{L}}/G_{\mathrm{T}}| = 1$. For $\sin\theta_{\mathrm{LT}} < 0$ the decay process acts as a source of a negative (positive) Collins effect for the fastest (slowest) decay product, as illustrated by the dashed contours in Fig. 5(b). For the fastest decay pion this contribution adds destructively with the Collins effect inherited from the ρ and gains over it, giving an overall negative analyzing power. The inverse is true for $\sin\theta_{\mathrm{LT}} > 0$ (continuous contour in Fig. 5).

Concerning the p_{T} dependence (right panel of Fig. 17) the largest effects can be seen for $p_{\mathrm{T}} < 0.5$ (GeV/c).

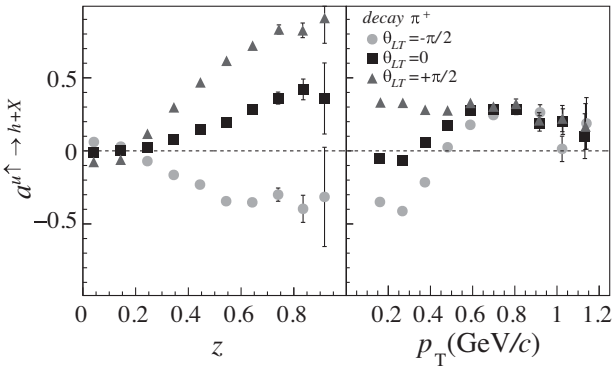

FIG. 17. Collins analyzing power for π^+ mesons produced in ρ^+ decays with $\theta_{\mathrm{LT}} = -\pi/2$ (full circles), $\theta_{\mathrm{LT}} = 0$ (squares), and $\theta_{\mathrm{LT}} = +\pi/2$ (triangles). We have taken $|G_{\mathrm{L}}/G_{\mathrm{T}}| = 1$.

Decay pions of this domain are mostly emitted with relative transverse momenta opposite to that of the ρ mesons. Besides the cut $z > 0.2$ selects mainly pions of positive p_z^*. Then, for $\sin\theta_{\mathrm{LT}} < 0$, looking at the orientations of the dotted ellipses in Fig. 5(b), one guesses that the pion momentum $\mathbf{p}_{\mathrm{T}}^*$ in the ρ rest frame is most often on the side opposite to the ρ one. Assuming the dominance of the first term in Eq. (34), $\mathbf{p}_{\mathrm{T}}(\pi)$ also is on the side opposite to $\mathbf{p}_{\mathrm{T}}(\rho)$. This explains the negative analyzing power of π^+ at not too large $\mathbf{p}_{\mathrm{T}}$. As for large $\mathbf{p}_{\mathrm{T}}$, they are mainly obtained when $\mathbf{p}_{\mathrm{T}}^*$ and $\mathbf{p}_{\mathrm{T}}(\rho)$ are on the same side, thus producing a positive analyzing power. The Wigner rotation increases this effect by making the major axis of the dashed ellipse nearly perpendicular to the $\hat{\mathbf{z}}$ axis. For $\sin\theta_{\mathrm{LT}} > 0$, according to Fig. 5, the cut $z > 0.2$ mainly rejects the $\mathbf{p}_{\mathrm{T}}^*$, which are opposite to $\mathbf{p}_{\mathrm{T}}(\rho)$, explaining the positive analyzing power at all $p_{\mathrm{T}}(\pi)$.

The sensitivity to $|G_{\mathrm{L}}/G_{\mathrm{T}}|$ and θ_{LT} of the Collins analyzing power for all the final pions, with all VMs decays, is shown in Fig. 18. As can be seen the overall effect of vector meson is stronger for favored fragmentation and weaker for unfavored fragmentation. In particular the z dependence of the π^+ analyzing power is no more linear for

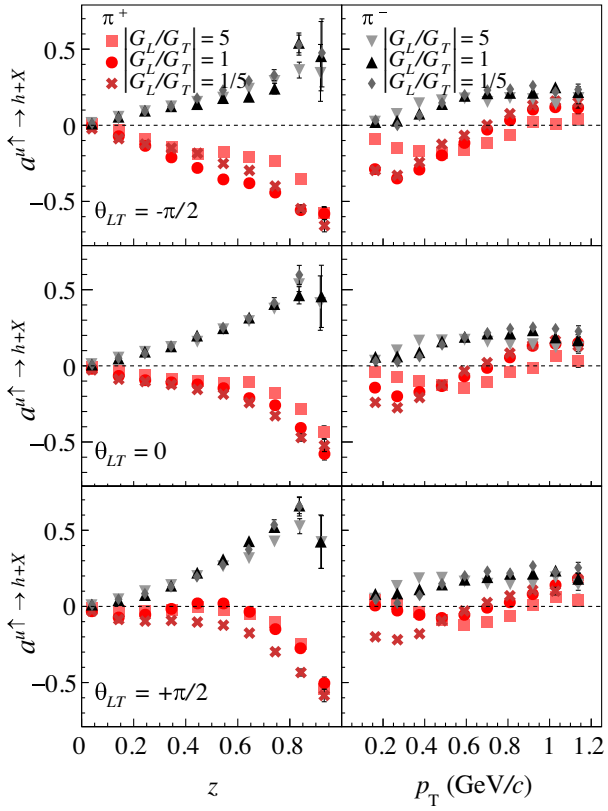

FIG. 18. Collins analyzing power for π^+ and π^- mesons as function of z (left panel) and of p_{T} (right panel) for $\theta_{\mathrm{LT}} = -\pi/2$ (upper row), $\theta_{\mathrm{LT}} = 0$ (middle row), and $\theta_{\mathrm{LT}} = +\pi/2$ (lower row). For each value of θ_{LT} the analyzing power is calculated for $|G_{\mathrm{L}}/G_{\mathrm{T}}| = 5$, $|G_{\mathrm{L}}/G_{\mathrm{T}}| = 1$ and $|G_{\mathrm{L}}/G_{\mathrm{T}}| = 1/5$.

both π^+ and π^- as it was in M19. The positive value of $\sin\theta_{\mathrm{LT}}$ strongly decreases the size of the π^+ analyzing power and increases the size of the π^- analyzing power. As function of p_{T} the effect of changing the parameters is large for π^+ in the small p_{T} region, as expected from Fig. 17, whereas for π^- only small differences can be seen.

Summarizing, variations in the free parameters $|G_{\mathrm{L}}/G_{\mathrm{T}}|$ and θ_{LT} produce large effects on the Collins analyzing power of the observed pions, and changes in $|G_{\mathrm{L}}/G_{\mathrm{T}}|$ can be competed by different choices of θ_{LT}. Precise measurements would allow us to fix their values.

V. A NEW DIHADRON TRANSVERSE SPIN ASYMMETRY

As mentioned in Sec. II B, vector meson decays do not contribute to the dihadron asymmetry if in Eq. (58) h_1 is taken as the h^+ of a h^+h^- pair (or the $h^\pm$ of a $h^\pm h^0$ pair) due to parity invariance. This is not true when h_1 is taken to be the fastest hadron of the pair, namely the hadron such that $z_1 > z_2$. In this case a dihadron asymmetry may appear, related to the oblique polarization of the vector meson, more precisely to the element $\hat{\rho}^{npl}_{\mathrm{XZ}}$ of the density matrix in the $\{\mathbf{X}, \mathbf{Y}, \mathbf{Z}\}$ basis of the null plane frame. We refer to this asymmetry as to the *z-ordered dihadron asymmetry*. $\hat{\rho}^{npl}$ deduces from the density matrix in the LR symmetric frame by the Wigner rotation $\hat{\rho}^{npl} = \mathcal{R}_{\mathbf{N}}(-\alpha_{\mathrm{W}\infty})\hat{\rho}\mathcal{R}_{\mathbf{N}}(\alpha_{\mathrm{W}\infty})$. The angular distribution of $\mathbf{R}$ is given by Eq. (39), replacing $\hat{\mathbf{r}}$ by $\hat{\mathbf{R}} = \mathbf{R}/|\mathbf{R}|$ and $\hat{\rho}$ by $\hat{\rho}^{npl}$. The z-ordered dihadron asymmetry is measured by $2\langle\sin(\phi_R - \phi_{\mathbf{S}_{q_A}})\rangle/|\mathbf{S}_{q_A\mathrm{T}}|$ with the restriction $R_z > 0$. It occurs between the primary mesons as well.

The simulated asymmetry is shown in Fig. 19 for pions produced in ρ^0 decay as function of the fractional energy of the pair z_{12}. The same cuts as in the standard dihadron asymmetry have been applied. For $\sin\theta_{\mathrm{LT}} \neq 0$, the large negative and positive asymmetries shown in the left and right panels are mainly due to the oblique polarization term $\sin\theta_{\mathrm{LT}} S_Y$ in $\mathrm{Re}\hat{\rho}_{\mathrm{XZ}}$ [see Eq. (B2)]. When going to $\mathrm{Re}\hat{\rho}^{npl}$ the Wigner rotation is, on average, not strong enough to change the sign of the XZ component. As can be seen the

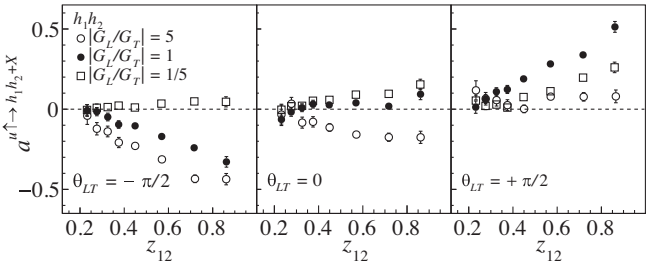

FIG. 19. Results for the analyzing power of the z-ordered dihadron asymmetry as function of the fractional energy z_{12} of the $\pi^+\pi^-$ pair produced in ρ^0 decay for the different values of θ_{LT} and $|G_{\mathrm{L}}/G_{\mathrm{T}}|$.

largest positive asymmetry is obtained for $|G_L/G_T| = 1$ and $\theta_{LT} = +\pi/2$. The combination $|G_L/G_T| = 5$ and $\theta_{LT} = -\pi/2$ gives also an asymmetry of the same size but with opposite sign.

The small dihadron asymmetry shown in the middle panel of Fig. 19 for $\theta_{LT} = 0$ and $|G_L/G_T| = 1$ requires another explanation. Indeed, with this choice of parameters it can be seen from Eq. (33) that there is no oblique polarization in the LR symmetric rest frame. There is however a nonvanishing $\hat{\rho}_{mn}$ element which, after the Wigner rotation, produces $\hat{\rho}^{npl}_{XZ} < 0$ in the null-plane frame. Combined with $R_z > 0$ this produces the small positive asymmetry at large z shown in Fig. 19 for $\theta_{LT} = 0$ and $|G_L/G_T| = 1$. The change of sign of the asymmetry at small z is instead due to the cuts $z_1 > 0.1$ and $z_2 > 0.1$.

For $|G_L/G_T| \neq 1$ but $\sin\theta_{LT} = 0$ the matrix element $\hat{\rho}^{npl}_{XZ}$ receives, by the Wigner rotation, a contribution from $\rho_{mm} - \rho_{ll} \propto |G_L|^2 - |G_T|^2$ responsible for the negative (positive) asymmetry for $|G_L/G_T| = 5$ (1/5).

It has been checked that the sensitivity to the free parameters as well as the size of the asymmetry remains still large when the z-ordered dihadron asymmetry is evaluated by using all final state hadron pairs in the ρ^0 mass region. Thus the z-ordered dihadron asymmetry depends strongly on the free parameters. The measurement of this asymmetry in SIDIS or e^+e^- annihilation would help to understand whether vector mesons produced in polarized fragmentation processes possess oblique polarization and to determine the values of the free parameters $|G_L/G_T|$ and θ_{LT}.

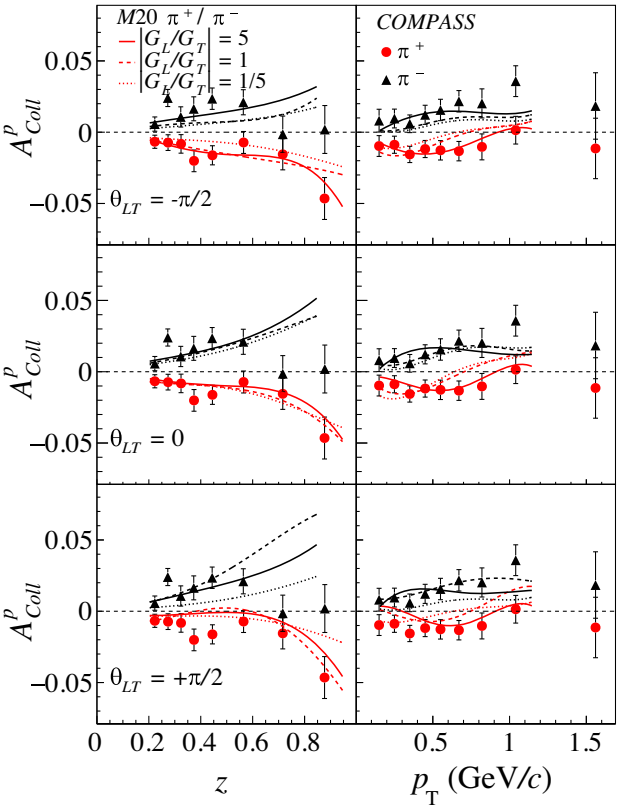

FIG. 20. Comparison between the scaled simulated Collins analyzing power for π^+ and π^- mesons (curves) and the Collins asymmetry as measured by COMPASS [5] (points) as function of z (left panel) and of p_T (right panel) for different combinations of $|G_L/G_T|$ and θ_{LT}.

VI. COMPARISON WITH EXISTING DATA

In order to get hints on the values of the free parameters $|G_L/G_T|$ and θ_{LT} we have compared the model results for fully polarized u quarks with the transverse spin asymmetries measured in SIDIS and in e^+e^- annihilation. In particular we compare the simulated asymmetries with the COMPASS results of Refs. [5,39], which are also in good agreement with the HERMES results [3,40]. Concerning the e^+e^- measurements we compare with the Collins asymmetries measured for oppositely charged back-to-back pions in e^+e^- annihilation to hadrons at BELLE [7], which are similar to the measurements performed by *BABAR* [41] and BESIII [42].

A. SIDIS

Figure 20 shows the comparison between the Collins analyzing power for charged pions as obtained from simulations with the Collins asymmetries measured by COMPASS [5]. In experiments, quarks are only partially polarized, following the transversity distribution [see Eq. (2)]. To take into account this fact, for each combination of the free parameters the MC results have been scaled by a constant factor λ estimated by a χ^2 minimization procedure using the simulated and measured asymmetries for π^- as function of p_T. The factor λ is similar for the different combinations of the free parameters and generally larger (up to a factor of two) than the value used for M18 in Ref. [21], due to the fact that in M20 the average Collins analyzing power is decreased as a consequence of the introduction of vector mesons. This difference can be recovered by increasing $\mathrm{Im}\mu$ by a factor of two while keeping $|\mu|^2$ constant.

All in all, given the small differences of the analyzing power for different parameter settings as compared to the experimental precision, no pair of values could be chosen. To exclude some combinations, a χ^2 test at 5% significance level considering the π^+ and π^- asymmetries as function of z, and the π^+ asymmetry as function of p_T has been performed. For the test, the last two z bins have been excluded since the trend at large z is expected to change in simulations of SIDIS events where a realistic mixture of the fragmenting quark flavors is considered [43]. We find that the test is passed by only three combinations of $|G_L/G_T|$ and θ_{LT}: $|G_L/G_T| = 5$ with $\theta_{LT} = -\pi/2$ or 0 and $|G_L/G_T| = 1$ with $\theta_{LT} = 0$.

Concerning dihadron asymmetries, the comparison between the simulated dihadron analyzing power and the

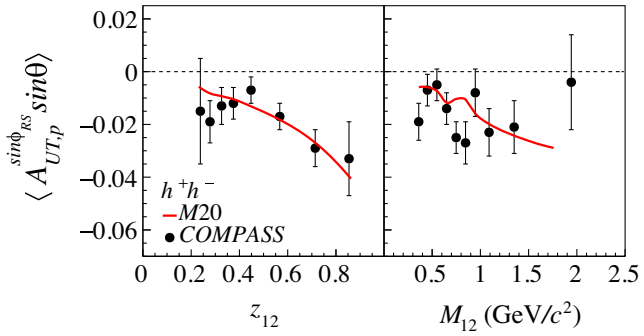

FIG. 21. Comparison between the scaled simulated dihadron analyzing power for h^+h^- pairs (curve) and the dihadron asymmetry measured by COMPASS [39] (points), as function of z_{12} (left panel) and of the invariant mass (right panel). $G_L \equiv G_T$ case.

corresponding asymmetries measured by COMPASS [39] is given in Fig. 21. The asymmetries are shown as functions of z_{12} and of the invariant mass M_{12}. The sensitivity of the dihadron analyzing power on the new parameters is small compared to the uncertainties of data, and in the figure only the results of the simulations obtained with $|G_L/G_T| = 1$ and $\theta_{LT} = 0$ have been used. Also the same scale factor as for the Collins asymmetry has been taken. The comparison is satisfactory apart from the invariant mass dependence in the ρ^0 region where the trend of the simulated analyzing power seems to be opposite to the data. This could be due to the fact that in the current model we have neglected the interference between amplitudes for the resonant and direct productions of oppositely charged hadron pairs [12,14,44,45].

Recent measurement of the Collins asymmetries for ρ^0 mesons produced inclusively in SIDIS on protons has been performed by COMPASS in Ref. [46]. The p_T dependence is similar to our simulated results for $|G_L/G_T| = 5$, up to large statistical uncertainties coming from the combinatorial background under the ρ^0 invariant mass peak.

B. e^+e^- annihilation

We consider now the A_{12}^{UL} asymmetry as measured by BELLE for back-to-back charged pions in the annihilation process $e^+e^- \to q\bar{q} \to h_1h_2 + X$ [7]. A_{12}^{UL} asymmetry is related to a_{12}, introduced in Eq. (3), by $A_{12}^{UL} = a_{12}^U - a_{12}^L$ where the superscript U refers to pairs of pions with unlike charges ($h_1h_2 = \pi^+\pi^-$ or $h_1h_2 = \pi^-\pi^+$) and L refers to pairs of pions with like charges ($h_1h_2 = \pi^+\pi^+$ or $h_1h_2 = \pi^-\pi^-$). Experimentally, A_{12}^{UL} corresponds to the amplitude of the $\cos(\phi_1 + \phi_2)$ modulation in the ratio $(1 + a_{12}^U \cos(\phi_1 + \phi_2))/(1 + a_{12}^L \cos(\phi_1 + \phi_2))$ between the normalized yields for unlike and like charge pion pairs, and is practically equivalent to $a_{12}^U - a_{12}^L$. ϕ_1 and ϕ_2 are the azimuthal angles of h_1 and h_2 about the thrust axis, measured from the plane defined by this axis and the e^- beam (the thrust axis approximates the $q\bar{q}$ axis).

We restrict ourselves to the case $z_1 = z_2 = z$ and $p_{1T} = p_{2T} = p_T$. The asymmetry can be written as

$$A_{12}^{UL}(z, p_T) = \langle \hat{a}_{NN} \rangle \times |a^{fav}(z, p_T)|^2 \times \left(\frac{5 + 5\alpha^2 + 2\alpha'^2}{5 + 5\beta^2 + 2\beta'^2} - \frac{5\alpha + \alpha'^2}{5\beta + \beta'^2} \right). \quad (59)$$

It includes the sum over the light quark flavors $q = u, d, s$. The quantities $\alpha = H_1^{unf}/H_1^{fav}$, $\alpha' = H_{1,s}^{unf}/H_1^{fav}$, $\beta = D_1^{unf}/D_1^{fav}$, and $\beta' = D_{1s}^{unf}/D_1^{fav}$ depend on z and the transverse momentum p_T with respect to the thrust axis. By using isospin and charge conjugation invariance the favored FF (fav) is defined as $D_1^{fav} = D_{1u}^{\pi^+} = D_{1\bar{u}}^{\pi^-} = D_{1d}^{\pi^-} = D_{1\bar{d}}^{\pi^+}$ and similarly for the Collins function. Instead, the unfavored FF (unf) is defined as $D_1^{unf} = D_{1u}^{\pi^-} = D_{1\bar{u}}^{\pi^+} = D_{1d}^{\pi^+} = D_{1\bar{d}}^{\pi^-}$ for u or d quarks, and $D_{1,s}^{unf} = D_{1s}^{\pi^+} = D_{1s}^{\pi^-} = D_{1\bar{s}}^{\pi^+} = D_{1\bar{s}}^{\pi^-}$ for s quarks (and similarly for the unfavored Collins function). a^{fav} is the Collins analyzing power for the favored fragmentation. $\langle \hat{a}_{NN} \rangle = \langle \sin^2\theta \rangle / \langle 1 + \cos^2\theta \rangle$ [8] where the θ is the angle between the e^- beam and the thrust axis.

The A_{12}^{UL} asymmetry measured by the BELLE collaboration is shown in Fig. 22 as functions of z and of p_T. It has been corrected for the charm contribution by using the charm contamination factors provided by BELLE and assuming vanishing Collins asymmetries in events initiated by charm quarks [7]. In the figure, the curves are the result of Eq. (59) evaluated using the fragmentation functions obtained from the simulated fragmentations of fully transversely polarized u and s quarks with $|G_L/G_T| = 5, 1, 1/5$, $\theta_{LT} = -\pi/2, 0, +\pi/2$, and the value $\langle \hat{a}_{NN} \rangle = 0.91$ provided in Ref. [7]. The simulation results have not been rescaled in this case. Each row refers to a different value of θ_{LT}. In each row the curves show the asymmetries from the simulations with different values of $|G_L/G_T|$. The kinematic cut $z > 0.1$ has been applied when looking at the asymmetry as function of z, and the cuts $z > 0.2$ and $p_T > 0.1$ GeV/c have been applied when looking at the asymmetry as function of p_T, as in the BELLE analysis. Also, following the BELLE analysis, the cut $\alpha_O < 0.3$ is applied on the opening angle α_O of the hadrons with respect to the string axis. This cut is relevant for the p_T dependence of the asymmetry and has practically no effect when looking at the asymmetry as function of z.

As can be seen from Fig. 22, the simulated asymmetries are in satisfactory agreement with the BELLE measurements as function of z and of p_T for the combinations $|G_L/G_T| = 5$ and $\theta_{LT} = -\pi/2$, except for the last point in z, and for $|G_L/G_T| = 1$ and $\theta_{LT} = 0$. This is consistent with the comparison with SIDIS measurements of the Collins asymmetries. For $|G_L/G_T| = 5$ and $\theta_{LT} = -\pi/2$

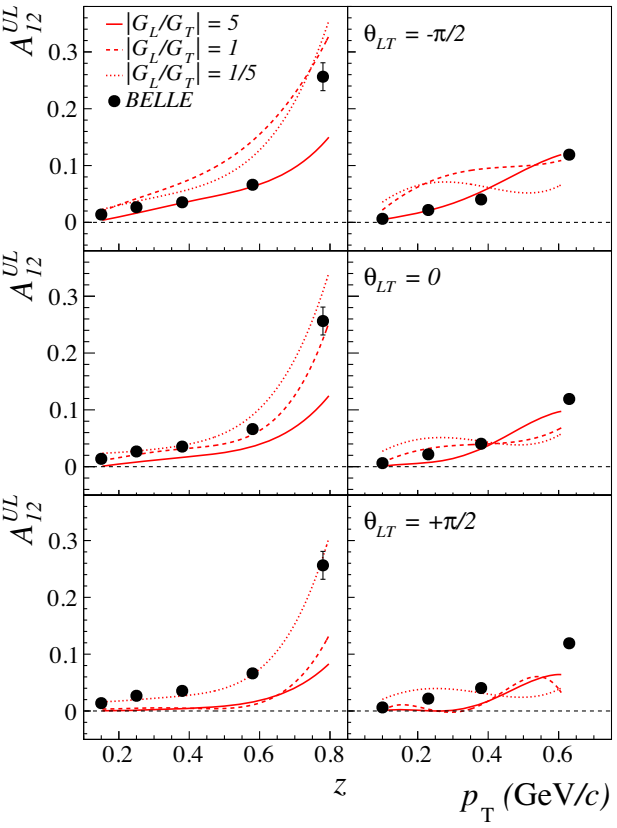

FIG. 22. Comparison between the e^+e^- Collins asymmetry A_{12} as measured by BELLE [7] (full points) as function of z (left panel) and of p_T (right panel), and the calculated Collins asymmetry from the simulation results for different values of the free parameters θ_{LT} and $|G_L/G_T|$ (curves).

quarks would couple preferentially to vector mesons with longitudinal polarization along the string axis but with some oblique polarization. Instead, for $|G_L/G_T| = 1$ and $\theta_{LT} = 0$ there is no preference for transversely or longitudinally polarized vector mesons and these would not have oblique polarization in the LR symmetric frame.

VII. CONCLUSIONS

Vector meson production in the polarized quark fragmentation process has been studied within the recursive string + $^3P_0$ model and the new model M20 has been developed. It improves the previous version (M19) by treating both vector and pseudoscalar meson emissions. It preserves the LR symmetry and the quantum mechanical properties like positivity and entanglement. The production of longitudinally and transversely polarized vector mesons in the LR symmetric frame has been implemented by introducing two different couplings to quarks of complex coupling constants G_L and G_T. To this aim, the new parameters $|G_L/G_T|$ and θ_{LT} have been added to the complex mass parameter μ already present in the model M19. Both $|G_L/G_T|$ and θ_{LT} enter the spin density matrix of the vector mesons producing angular modulations in the distribution of the decay products. The Wigner rotation relating the LR symmetric frame and the null-plane frame, where the decay products are recorded, has been studied.

M20 has been implemented in a stand alone Monte Carlo program which allowed to perform detailed simulations of the fragmentation process. We have found that the quark spin degree of freedom enters both the kinematic distributions (*hidden-spin* effects) and the spin dependent quantities like the Collins and dihadron asymmetries. The Collins asymmetries of vector mesons turns out to be opposite to their pseudoscalar analogs for the favored fragmentation and strongly dependent on the $|G_L/G_T|$ parameter.

The contribution of the decay hadrons to the Collins asymmetry has also been studied and found to depend on the oblique polarization of the vector meson, which is governed by the parameter θ_{LT}. The oblique polarization has also a relevant role in the z-ordered dihadron asymmetry, proposed here but not yet measured. Future precise measurements of these asymmetries in SIDIS will allow a better estimate of the free parameters of the model and more safe predictions.

Finally, the simulation results on the Collins and the dihadron asymmetries have been compared to the SIDIS and e^+e^- annihilation data finding an encouraging similarity. The precision of the existing experimental data, however, does not allow us to fix the values of the free parameters but give some indication that the values $|G_L/G_T| \geq 1$ and $\theta_{LT} \leq 0$ are the preferred ones, namely that quarks may couple preferentially to longitudinally polarized vector mesons with oblique polarization in the LR symmetric frame.

To summarize, this new version of the string + $^3P_0$ model with vector meson production is rich in the predicted phenomena, like the oblique polarization and the hidden spin effects, and it is successful in the description of the experimental data.

ACKNOWLEDGMENTS

We would like to thank Franco Bradamante for his support and encouragement, and John Collins and Torbjörn Sjöstrand for the interesting and useful discussions. The work of A. Kerbizi has also been supported by the European Union Horizon 2020 research and innovation program under Grant Agreement No. 824093 (STRONG-2020).

APPENDIX A: THE POLARIZATION ELLIPSOID

In the decay of a vector meson in two pseudoscalar mesons, the angular distribution of the decay products is given by

$$d\mathcal{N}(\hat{\mathbf{r}})/d\Omega = \frac{3}{4\pi} A^2(\hat{\mathbf{r}}),$$
$$A^2(\hat{\mathbf{r}}) = \hat{r}_\alpha \hat{\rho}_{\alpha\alpha'}(h) \hat{r}_{\alpha'}, \qquad \text{(A1)}$$

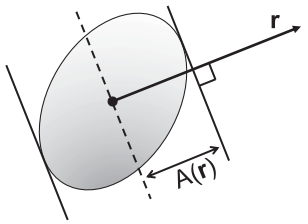

FIG. 23. Polarization ellipsoid of a vector meson.

where $\hat{\rho}_{\alpha\alpha'}$ is the density matrix of the VM, $\mathbf{r}$ the relative momentum of the decay mesons and $\hat{\mathbf{r}} = \mathbf{r}/|\mathbf{r}|$. One can replace $\hat{\rho}_{\alpha\alpha'}$ by the tensor polarization matrix $\mathrm{Re}\hat{\rho}_{\alpha\alpha'}$. From this matrix on can build the *polarization ellipsoid*, whose symmetry axes are along the eigenvectors, with half lengths equal to the square roots of the eigenvalues. It is the dual of the ellipsoid $r_\alpha \hat{\rho}_{\alpha\alpha'} r_{\alpha'} = 1$ in the polar reciprocal transformation. This is the 3D generalization of the polarization ellipse of photons.

$A(\hat{\mathbf{r}})$ is obtained geometrically as shown in Fig. 23: the distance between two planes orthogonal to $\hat{\mathbf{r}}$ and tangential to the ellipsoid is $2A(\hat{\mathbf{r}})$. The projection of the ellipsoid on, for instance, the (x, y) plane is the *polarization ellipse* associated to the 2×2 reduced matrix of elements $\mathrm{Re}\hat{\rho}_{xx}$, $\mathrm{Re}\hat{\rho}_{xy}$, $\mathrm{Re}\hat{\rho}_{yx}$, and $\mathrm{Re}\hat{\rho}_{yy}$.

APPENDIX B: THE FULL VM DENSITY MATRIX

Including the imaginary, antisymmetric part of the VM density matrix, Eq. (33) generalizes as

$$\begin{aligned}
\hat{\rho}_{\mathrm{ll}} &= (1 - \hat{a}S_n)|G_{\mathrm{L}}|^2/N(\mathbf{S}),\\
\hat{\rho}_{\mathrm{mm}} &= (1 - \hat{a}S_n)|G_{\mathrm{T}}|^2/N(\mathbf{S}),\\
\hat{\rho}_{\mathrm{nn}} &= (1 + \hat{a}S_n)|G_{\mathrm{T}}|^2/N(\mathbf{S}),\\
\hat{\rho}_{\mathrm{ml}} &= i(-S_n + \hat{a})G_{\mathrm{T}}G_{\mathrm{L}}^*/N(\mathbf{S}) = (\hat{\rho}_{\mathrm{lm}})^*,\\
\hat{\rho}_{\mathrm{mn}} &= (iS_l - \hat{a}S_m)|G_{\mathrm{T}}|^2/N(\mathbf{S}) = (\hat{\rho}_{\mathrm{nm}})^*,\\
\hat{\rho}_{\mathrm{nl}} &= (-iS_m + \hat{a}S_l)G_{\mathrm{T}}G_{\mathrm{L}}^*/N(\mathbf{S}) = (\hat{\rho}_{\mathrm{ln}})^*.
\end{aligned} \tag{B1}$$

Note.—If $|\mathbf{S}_q| = 1$, then $\hat{\rho}$ is a matrix of rank 2 (i.e., $\det\hat{\rho} = 0$). Indeed, its rank is bounded by the rank of $\hat{\rho}(q)$, which is 1, times the rank of the acceptance matrix $\check{\rho}(q')$, which is 2 as long as the fragmentation of q' has not yet been performed by the simulation.

The real part of $\hat{\rho}$ in the $\{\mathbf{X}, \mathbf{Y}, \mathbf{Z}\}$ basis linked to the quark transversity (i.e., $S_X = 0$) is

$$\begin{aligned}
\hat{\rho}_{\mathrm{ZZ}} &= (1 + \hat{a}m_X S_Y)|G_{\mathrm{L}}|^2/N(\mathbf{S}),\\
\hat{\rho}_{\mathrm{XX}} &= (1 + \hat{a}m_X S_Y)|G_{\mathrm{T}}|^2/N(\mathbf{S}),\\
\hat{\rho}_{\mathrm{YY}} &= (1 - \hat{a}m_X S_Y)|G_{\mathrm{T}}|^2/N(\mathbf{S}),\\
\mathrm{Re}\hat{\rho}_{\mathrm{XY}} &= \hat{a}m_X S_Y|G_{\mathrm{T}}|^2/N(\mathbf{S}),\\
\mathrm{Re}\hat{\rho}_{\mathrm{XZ}} &= -[\sin\theta_{\mathrm{LT}}(S_Y + \hat{a}m_X)\\
&\quad + \cos\theta_{\mathrm{LT}}\hat{a}m_Y S_Z]|G_{\mathrm{L}}G_{\mathrm{T}}|/N(\mathbf{S}),\\
\mathrm{Re}\hat{\rho}_{\mathrm{YZ}} &= (-\sin\theta_{\mathrm{LT}}\hat{a}m_Y\\
&\quad + \cos\theta_{\mathrm{LT}}\hat{a}m_X S_Z)|G_{\mathrm{L}}G_{\mathrm{T}}|/N(\mathbf{S}).
\end{aligned} \tag{B2}$$

[1] A. Metz and A. Vossen, Prog. Part. Nucl. Phys. **91**, 136 (2016).
[2] J. C. Collins, Nucl. Phys. **B396**, 161 (1993).
[3] A. Airapetian *et al.* (HERMES Collaboration), Phys. Rev. Lett. **94**, 012002 (2005).
[4] V. Yu. Alexakhin *et al.* (COMPASS Collaboration), Phys. Rev. Lett. **94**, 202002 (2005).
[5] C. Adolph *et al.* (COMPASS Collaboration), Phys. Lett. B **744**, 250 (2015).
[6] X. Qian *et al.* (Jefferson Lab Hall A Collaboration), Phys. Rev. Lett. **107**, 072003 (2011).
[7] H. Li *et al.* (Belle Collaboration), Phys. Rev. D **100**, 092008 (2019).
[8] X. Artru and J. C. Collins, Z. Phys. C **69**, 277 (1996).
[9] A. Martin, F. Bradamante, and V. Barone, Phys. Rev. D **91**, 014034 (2015).
[10] M. Anselmino, M. Boglione, U. D'Alesio, J. O. Gonzalez Hernandez, S. Melis, F. Murgia, and A. Prokudin, Phys. Rev. D **92**, 114023 (2015).
[11] Z.-B. Kang, A. Prokudin, P. Sun, and F. Yuan, Phys. Rev. D **93**, 014009 (2016).
[12] J. C. Collins, S. F. Heppelmann, and G. A. Ladinsky, Nucl. Phys. **B420**, 565 (1994).
[13] R. L. Jaffe, X.-m. Jin, and J. Tang, Phys. Rev. Lett. **80**, 1166 (1998).
[14] A. Bianconi, S. Boffi, R. Jakob, and M. Radici, Phys. Rev. D **62**, 034008 (2000).
[15] O. Nachtmann, Nucl. Phys. **B127**, 314 (1977).
[16] A. V. Efremov, L. Mankiewicz, and N. A. Tornqvist, Phys. Lett. B **284**, 394 (1992).
[17] T. B. Hayward *et al.*, Phys. Rev. Lett. **126**, 152501 (2021).
[18] X. Artru, in *Proceedings of XIII Advanced Research Workshop on High Energy Spin Physics (DSPIN-09), Dubna, 2009*, edited by A. Efremov and S. Goloskokov (JINR., Dubna, 2009), pp. 33–40.
[19] X. Artru, in *Proceedings of XIV Advanced Research Workshop on High Energy Spin Physics (DSPIN-11)*, edited by A. Efremov and S. Goloskokov (JINR., Dubna, 2011), pp. 45–52.
[20] X. Artru and Z. Belghobsi, in *XV Advanced Research Workshop on High Energy Spin Physics*, edited by

A. Efremov and S. Goloskokov (Dubna, Russia, 2013), pp. 33–40.
[21] A. Kerbizi, X. Artru, Z. Belghobsi, F. Bradamante, and A. Martin, Phys. Rev. D **97**, 074010 (2018).
[22] A. Kerbizi, X. Artru, Z. Belghobsi, and A. Martin, Phys. Rev. D **100**, 014003 (2019).
[23] B. Andersson, G. Gustafson, G. Ingelman, and T. Sjostrand, Phys. Rep. **97**, 31 (1983).
[24] B. Andersson, G. Gustafson, and G. Ingelman, Phys. Lett. **85B**, 417 (1979).
[25] T. Sjostrand, S. Mrenna, and P. Z. Skands, J. High Energy Phys. 05 (2006) 026; Comput. Phys. Commun. **178**, 852 (2008).
[26] A. Kerbizi and L. Lönnblad, arXiv:2105.09730.
[27] J. Czyzewski, Acta Phys. Pol. **27**, 1759 (1996).
[28] A. Kerbizi, Recursive fragmentation of a polarized quark, Ph.D. thesis, Trieste U., 2020.
[29] J. C. Collins, Nucl. Phys. **B304**, 794 (1988).
[30] I. G. Knowles, Nucl. Phys. **B310**, 571 (1988).
[31] X. Artru and G. Mennessier, Nucl. Phys. **B70**, 93 (1974).
[32] M. T. Tanabashi *et al.* (Particle Data Group), Phys. Rev. D **98**, 030001 (2018).
[33] A. A. Minaenko *et al.*, Z. Phys. C **62**, 15 (1994).
[34] H. Leutwyler and J. Stern, Ann. Phys. (N.Y.) **112**, 94 (1978).
[35] X. Artru, M. Elchikh, J.-M. Richard, J. Soffer, and O. V. Teryaev, Phys. Rep. **470**, 1 (2009).
[36] A. Bacchetta and P. J. Mulders, Phys. Rev. D **62**, 114004 (2000).
[37] M. Aghasyan *et al.* (COMPASS Collaboration), Phys. Rev. D **97**, 032006 (2018).
[38] C. Adolph *et al.* (COMPASS Collaboration), Phys. Lett. B **753**, 406 (2016).
[39] C. Adolph *et al.* (COMPASS Collaboration), Phys. Lett. B **736**, 124 (2014).
[40] A. Airapetian *et al.* (HERMES Collaboration), J. High Energy Phys. 06 (2008) 017.
[41] J. P. Lees *et al.* (*BABAR* Collaboration), Phys. Rev. D **90**, 052003 (2014).
[42] M. Ablikim *et al.* (BESIII Collaboration), Phys. Rev. Lett. **116**, 042001 (2016).
[43] A. Kerbizi and L. Lönnblad, Proc. Sci. DIS2019 (**2019**) 179 [arXiv:1909.02280].
[44] J. C. Collins and G. A. Ladinsky, arXiv:hep-ph/9411444.
[45] A. Bacchetta and M. Radici, Phys. Rev. D **74**, 114007 (2006).
[46] A. Kerbizi (COMPASS Collaboration), *Contribution to the 28th International Workshop on Deep Inelastic Scattering and Related Subjects* (2021), arXiv:2107.10099.